Periodic Phase Separation: A Numerical Study via a Modified Cahn-Hilliard Equation

by

Ping Zhang

B.Sc., Jilin University, China, 2003

A THESIS SUBMITTED IN PARTIAL FULFILLMENT
OF THE REQUIREMENTS FOR THE DEGREE OF
MASTER OF SCIENCE
IN THE DEPARTMENT
OF
MATHEMATICS

SIMON FRASER UNIVERSITY
Summer 2006

APPROVAL

Name: Ping Zhang

Degree: Master of Science

Title of thesis: Periodic Phase Separation: A Numerical Study via a Modified Cahn-Hilliard Equation

Examining Committee: Dr. Ralf Wittenberg
Chair

Dr. Rustum Choksi
Senior Supervisor

Dr. Mary Catherine Kropinski
Supervisor

Dr. JF Williams
Examiner

Date Approved: August 2, 2006

Abstract

In this thesis, we investigate a model for periodic phase separation. The model consists primarily of a modified Cahn-Hilliard equation which is simply a gradient flow for a nonlocal energy functional. This functional was introduced to model microphase separation of diblock copolymers. Numerical experiments are performed, both to test certain hypotheses as well as to explore the complex energy landscape of the nonlocal functional. The numerical method used is a split-step pseudo-spectral method. We solve the modified Cahn-Hilliard equation in two steps: first we solve the linear part of the equation and then advance the solution according to the nonlinear part. The nonlinear term is treated pseudo-spectrally.

Acknowledgments

Thanks, first of all, go to my supervisor Dr. Rustum Choksi for his continuing guidance through my graduate studies. His support, kindness, research ideas as well as his careful reading of this thesis are extremely appreciated.

I would like to thank Dr. Dave Muraki and Dr. Ralf Wittenberg, who gave me a lot of helpful suggestions when I first came to the Department of Mathematics.

I would also like to thank Dr. Juan Restrepo for helping me understand the numerical aspects related to this thesis and introducing me to the use of the UNIX system. I really appreciate his humor and patience. The code used in this thesis incorporates earlier work of his.

Last but not least, I would like to thank all the graduate students in the Department of Mathematics, who made my life and study here interesting, colourful and memorable.

Dedication

To my Mother.

Contents

List of Tables

List of Figures

Chapter 1

Introduction

1.1 Periodic Phase Separation

According to experiments, many physical systems exhibit periodic phase separation (Figure 1.1) on a fixed scale which is much less than the sample size. Depending on the composition, different periodic structures have been observed, like lamellar, spheric, cylindric and gyroid (shown in Figure 1.1). A density functional theory, first introduced by Ohta & Kawasaki ([16]) to study the microphase separation of diblock copolymer, entails the minimization of a free energy functional of nonlocal type. This functional takes the form:

$$\mathcal{F}(u) = \int_D \frac{\epsilon^2}{2}|\nabla u|^2 + W(u) + \frac{\sigma}{2}|(-\Delta)^{-\frac{1}{2}}(u-m)|^2 dx. \tag{1.1}$$

We refer to this functional as the nonlocal Cahn-Hilliard energy functional ([20] [21]), whereby the standard Cahn-Hilliard energy functional is augmented by a long-range interaction term. This term is proportional to an interaction material parameter related to the length of the copolymer chain. This nonlocal functional is a mathematical paradigm for energy-driven pattern formation associated with short and long-range interactions.

Heuristically, we know that minimization of the nonlocal term prefers oscillation. Thus it is reasonable that periodic or nearly periodic structures are expected to emerge as the value of σ increases. Actually, in one space dimension, the nonlocal Cahn-Hilliard

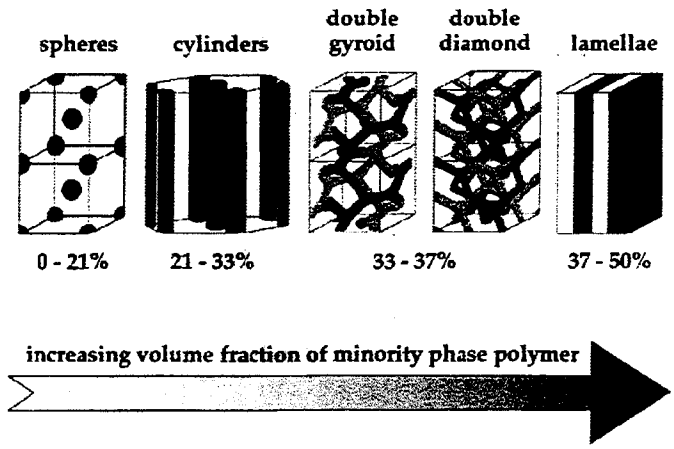

Figure 1.1: Periodic phase separation. Figure taken from reference [11]

functional reduces to a functional proposed by Müller ([18]) as a toy problem. It has been proven that its minimizers are periodic. In higher space dimensions, there is evidence to support the contention that minimizers are at least nearly periodic. However, the precise nature of the geometry of minimizers within a periodic cell remains an open problem.

Minimizing structures depend on different volume fractions m. In two dimensional phase separation, strips are expected for $m = 0$, while circles are expected for $m \neq 0$. When the role that σ plays is considered, we hope to see more strips or circles as the value of σ increases. Numerical experiments are performed to test these hypotheses. From the numerical results shown in Chapter 5, we will see how the value of m controls the minimizing structures and how σ affects the periodicity.

1.2 Thesis Layout

This thesis is organized as follows. We start in Chapter 2 by discussing the physical problem and the nonlocal Cahn-Hilliard energy functional. Where is it from? What is this equation for? What effects do the terms in energy have in minimization? We then briefly summarize the derivation of a density functional theory which was recently given by R. Choksi and X. Ren ([9]). The energy functional is derived as an offspring of the self-consistent mean field theory ([9]) and all parameters are connected to the fundamental material parameters.

In Chapter 3 we consider evolution equations induced from gradient flows. As we will see, under different Hilbert spaces, different evolution equations will be obtained from the nonlocal Cahn-Hilliard functional. But taking the physical aspect of the problem into account, only when a specific Hilbert space, namely $\dot{H}^{-1}$, which is the zero-average subspace of H^{-1}, is considered, the mass of the system is conservative. Under this Hilbert space, we arrive at the modified Cahn-Hilliard equation.

From Chapter 4, we will concentrate on the numerical aspects of this problem. The numerical method we use is the *Split-Step Pseudo-Spectral Method.* The evolution equation is the one under $\dot{H}^{-1}$, which conserves mass. This partial differential equation is separated into a linear part $\mathcal{L}u$ and a nonlinear part $\mathcal{N}(u)$. The linear and nonlinear equations are then solved in sequential order to approximate the solution of (3.15), in which the solution of one subproblem is employed as an initial condition for the next one. The fast Fourier transform is used for the spatial discretization, since we consider periodic boundary conditions. As for the cubic term in the nonlinear equation, we apply a pseudo-spectral method. Other numerical methods for Cahn-Hilliard equation and its nonlocal form can be found in [1], [4] and [14].

Numerical results in all three spatial dimensions are given in Chapter 5, in which the evolutionary procedures of phase separation and different minimizing structures related to the mean value m, as well as the role that σ plays, are clearly shown. We conclude in Chapter 6 with some remarks and future work.

Chapter 2

The Physical Paradigm and the Nonlocal Cahn-Hilliard Energy Functional

In this thesis we consider a free energy functional which was introduced to describe the microphase separation of diblock copolymers. The functional has a rescaled, nondimensional form as a function of u. It takes the following form:

$$\mathcal{F}(u) = \int_D \frac{\epsilon^2}{2}|\nabla u|^2 + W(u) + \frac{\sigma}{2}|(-\Delta)^{-\frac{1}{2}}(u-m)|^2 d\mathbf{x}, \tag{2.1}$$

where m denotes the average of u over D, i.e.,

$$m := \int_D u dx.$$

As we will explain later, u represents the density difference between the mass fractions of monomers A and B.

In this chapter, we examine the nonlocal energy functional (2.1) in some detail.

2.1 The Physical Problem

A physical paradigm for periodic phase separation is provided by microphase separation of diblock copolymers ([2]). The simplest and most studied structure is the linear AB diblock copolymer, which consists of a long sequence of type A monomers covalently linked to a chain of type B monomers (Figure 2.1 (a)). A homogeneous mixture (Figure 2.1 (b)) of AB diblock copolymers is usually formed at a relatively high temperature T_I, which is greater than the critical temperature T_c. At this high temperature, the binary mixture is stable with mean composition m. Suppose now that the temperature is quenched (rapidly reduced) to a temperature T_f, lower than T_c. Experimentally, one observes that the concentration u of the mixture changes from the uniform mixed state to that of spatially separated two-phase structure, denoted by I and II (Figure 2.1 (c) and (d)). It is known experimentally that the uniform mixture $u = m$ is very unstable, and that the growth of instabilities results in phase separation, during which some of the mixture becomes phase I with $u = u_1$, and the rest becomes phase II with $u = u_2$. The phase separation is on a mesoscopic scale, much less than the domain size of diblock copolymers. Macrophase separation, however, like the separation of water and oil, cannot happen because the chains of copolymers are chemically bonded.

The phase separation is observed to be periodic both numerically and theoretically. Different types of periodic structures depend on the composition. These ordered structures make diblock copolymers of great technological interest.

The remarkable property of diblock copolymers is their ability to self-assemble in the melt into a variety of ordered structures with mesoscale periodicities. These structures can be precisely controlled by varying, for example, the composition of the diblock copolymers or the segregation between blocks (via temperature or degree of polymerization). One of the strategic goals for these self-assembling materials is to experimentally control the resulting structures, which leads to their utilization in diversiform fundamental and technological applications including electron transport in confined and periodic geometries. The controllable architectures of these materials may lead to their use in electronic and magnetic microstructures via selective decoration of individual diblock

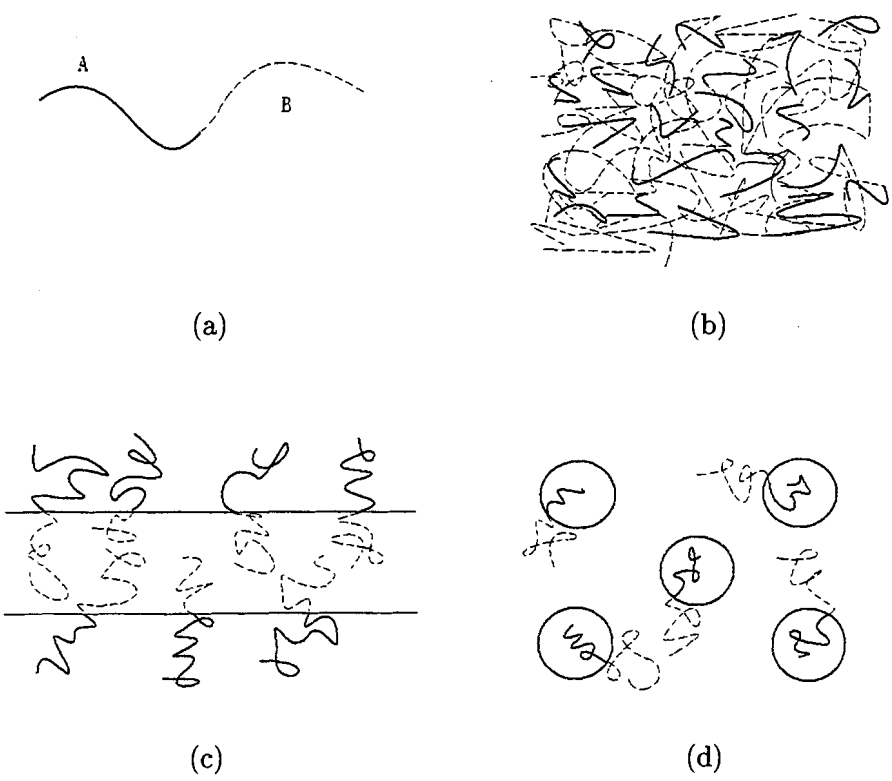

Figure 2.1: (a) A diblock copolymer molecule; (b) Above some temperature T_c, A and B subchains mix to make a uniform disordered phase; (c) Below temperature T_c, the subchains A and B begin to segregate into A-rich (phase I) and B-rich (phase II) regions in which the length of subchains is equal; (d) The subchains A and B begin to segregate into A-rich and B-rich regions in which the length of subchains is unequal.

components with either conductive or magnetic particles.

2.2 Cahn-Hilliard Energy Functional and the Related Equation

As an introduction to the nonlocal Cahn-Hilliard functional, let us give a brief review of Cahn-Hilliard energy functional and the related Cahn-Hilliard equation ([3] [4]) in this section.

In order to model the physical phenomenon of the phase separation discussed above, Cahn and Hilliard first introduced a free energy functional

$$\mathcal{F}(u) = \int_\Omega \frac{1}{2}\epsilon^2|\nabla u|^2 + W(u)dx \tag{2.2}$$

in 1958 ([5]). The first gradient term in this integral is a quantity representing the surface energy of the interfaces separating phases. $W(u)$ is a smooth and nonnegative function with two equal minima at $u = u_1$ and $u = u_2$. At this level, any double-well function would do.

The functional derivative of $\mathcal{F}(u)$ gives us the generalized potential Φ

$$\Phi = -\epsilon^2\Delta u + W'(u),$$

and the mass flux is given by $-\nabla\Phi$. Thus the evolution equation for the process of phase separation is

$$\frac{\partial u}{\partial t} = \nabla \cdot (\nabla\Phi),$$

which can be equivalently written as

$$\frac{\partial u}{\partial t} = \Delta(-\epsilon^2\Delta u + W'(u)). \tag{2.3}$$

This fourth order in space and nonlinear time-dependent partial differential equation is the well-known Cahn-Hilliard equation. This equation is supplemented with boundary conditions on the boundary $\partial\Omega$, which are normally taken as the natural boundary condition

$$\frac{\partial u}{\partial n} = 0 \qquad \text{on} \quad \partial\Omega$$

and the no mass flux condition

$$\frac{\partial \Phi}{\partial n} = 0 \qquad \text{on} \quad \partial\Omega.$$

The no mass flux boundary condition implies that the total amount of mass must remain constant, equal to the original amount. This means equation (2.3) is subject to the constraint, mass conservation,

$$\int_{\Omega} u(x,t)dx = m. \tag{2.4}$$

The simplest form of $W(u)$ having the double-well potential is

$$W(u) = \frac{1}{4}(1-u^2)^2.$$

It is in this form of W that the Cahn-Hilliard equation has been widely studied. In chapter 3 we will see how to obtain our modified Cahn-Hilliard equation as a gradient flow. The Cahn-Hilliard equation (2.3) conserves mass. This property will be shown in section 3.4.

2.3 The Nonlocal Cahn-Hilliard Energy Functional

Various mean field theories have been introduced to model and capture aspects of the process of phase separation. One of the most successful theories is the self-consistent mean field theory developed and applied over years. In this mean field theory the effect of monomer interactions is stimulated via external fields acting separately on the A and B monomers.

The Cahn-Hilliard energy functional of nonlocal type was introduced to describe the microphase separation of diblock copolymers. Mathematical results, however, pertaining to (2.1) can only be meaningful if they are complemented with an understanding of where this functional comes from. Originally this functional was derived by Ohta and Kawasaki ([16]) using the theory statistical mechanics. More recently, Choksi and Ren ([9]) re-examined the derivation of the Ohta-Kawasaki density functional theory and provided a detailed derivation of the nonlocal Cahn-Hilliard energy functional.

A summary of the main steps in deriving the energy functional is given here to show some idea of how such a functional can be obtained from statistical physics. Details are provided by [9]. The derivation, which is based on the statistical physics of block copolymer, contains three main steps. The first is what is known as the self-consistent mean field theory. The second step entails writing the free energy entirely in terms of the macrophase monomer density. And the last step is to reduce the functional to a scalar order parameter and derive the rescaled nonlocal Cahn-Hilliard functional.

The copolymer melt is modeled with a phase space of n continuous chains. Each chain r_i has N total monomers, and it is a Brownian process in the function space

$$\Gamma_i = C([0, N], R^3).$$

If we assume the Wiener measure of the Brownian motion is dP, then the space Γ_i is equipped with the measure $d\mu_s = dx \times dP$. Since there are n chains in the material, the space of diblock is

$$\Gamma = \{r = (r_1, ..., r_n) : r_i \in C([0, N], R^3)\}.$$

And the product measure is

$$d\mu = \prod_{j=1}^{n} d\mu_s.$$

The total number of monomers in the melt is nN. We let $I_A = [0, N_A]$ denote the interval occupied by the A-monomers and $I_B = [N_A, N]$ denote the interval occupied by the B-monomers. Then we introduce the Hamiltonian of this copolymer $H(r)$ as well as the associated Gibbs canonical distribution $D(r)$ and partition function Z. Finally, we can write the free energy of this system in terms of the partition function Z.

If we define the microscopic densities

$$\rho_A(x, r) = \sum_{i=1}^{n} \int_{I_A} \delta(x - r_i(\tau)) d\tau,$$

$$\rho_B(x, r) = \sum_{i=1}^{n} \int_{I_B} \delta(x - r_i(\tau)) d\tau,$$

then in terms of the microscopic densities $\rho(x,r)$, the macroscopic densities of the monomer units should be given by

$$\langle \rho_A(x) \rangle = \int_\Gamma \rho_A(x,r) D(r) d\mu,$$
$$\langle \rho_B(x) \rangle = \int_\Gamma \rho_B(x,r) D(r) d\mu,$$

and the Hamiltonian can be written as

$$H(r) = \int_\Omega \frac{V^{km}}{2\rho_0} \rho_k(x,r) \rho_m(x,r) dx,$$

where V^{km} represents the interaction parameters and is taken to be positive, and $\rho_0 = \frac{nN}{|\Omega|}$ is the average monomer number density. k and m take on the values of either A or B. There is an implied summation over k and m.

Because of the complexity of the interaction V^{km}, $\langle \rho_k(x) \rangle$ can not be obtained directly from the distribution D. A variational principle which the self-consistant mean field theory is based on, however, makes it possible to approximate the true free energy by a minimization over a class of distributions generated by a pair of external fields $U = (U^A, U^B)$, acting on the A and B monomers respectively. Then the Hamiltonian of this system is

$$H_U(r) = \sum_{i=1}^{n} \sum_k \int_{I_k} U^k(r_i(\tau)) d\tau.$$

The induced Gibbs cannonical distribution and partition fuunction are given by

$$D_U(r) = \frac{1}{Z_U} \exp(-\beta H_U(r)),$$
$$Z_U = \int_\Gamma \exp(-\beta H_U(r)) d\mu,$$

where β is the reciprocal of the absolute temperature with Boltzmann's constant taken to be 1. Taking into consideration the variational principle ([9]) which D satisfies,

$$\mathcal{F}(U) = \int_\Gamma H(r) D_U d\mu - \frac{S(D_U)}{\beta}$$

may be considered as an approximate free energy of the original system under the distribution D_U of the external fields. $S(D_U)$ denotes the statistical entropy associated with the distribution D_U, and is in the form

$$S(D_U) = \log Z_U + \beta \int_\Omega U^k(x)\eta_k(x)dx.$$

For convenience of notation, $\eta_k(x) = \langle \rho_k(x) \rangle_U$ is used to denote the expectations with respect to $D_U(r)d\mu$. We then rewrite the approximate free energy $\mathcal{F}$ as a functional of the external fields U:

$$\begin{aligned} \mathcal{F}(U) &= \int_\Omega \frac{V^{km}}{2\rho_0}\eta_k(x)\eta_m(x)dx - \frac{S(D_U)}{\beta} \\ &= \int_\Omega \left[\frac{V^{km}}{2\rho_0}\eta_k(x)\eta_m(x) - U^k(x)\eta_k(x)\right] dx - \frac{1}{\beta}\log Z_U. \end{aligned} \tag{2.5}$$

Now begins the second step whose main purpose is to write this free energy (2.5) entirely in terms of the macroscopic monomer densities $\eta_k(x)$. As we can see, the first term in (2.5) is already written in terms of the monomer densities. So we only need to turn the $-\frac{S(D_U)}{\beta}$ term in the free energy as a functional of $\eta_k(x)$.

Since the expectations $\eta_k(x)$ with respect to the external fields U are given by the solutions to the forward and backward parabolic differential equations associated with the Feynman-Kac integration theory, we can find $\eta_k(x)$, Z_U and most importantly $\mathcal{F}(U)$. With the help of calculating the derivative of $\mathcal{F}$ at U, one can find the following equation

$$\frac{\delta(-S(D_U))}{\delta(\eta)} = -\beta U. \tag{2.6}$$

Based on this equation, we can find $S(D_U)$ in terms of η_k by integrating βU, if βU can be written as a function of η_k. Actually βU can be expressed in terms of η_k through

$$\beta U^k(x) = -\frac{N}{\rho_0}\left(\frac{l^2}{6N}(-\Delta)K^{km} + \frac{6}{l^2N^3}(-\Delta)^{-1}L^{km}\right)(\eta_m - \bar{\eta}_m)(x). \tag{2.7}$$

In this expression,

$$K^{km} = \frac{1}{2}\begin{pmatrix} \frac{1}{a} & 0 \\ 0 & \frac{1}{1-a} \end{pmatrix}, L^{km} = \frac{3}{2}\begin{pmatrix} \frac{1}{a^2} & -\frac{1}{a(1-a)} \\ -\frac{1}{a(1-a)} & \frac{1}{(1-a)^2} \end{pmatrix},$$

and $a = N_A/N$ denotes the molecular weight of A monomer and l denotes the Kuhn statistical length which measures the average distance between two adjacent monomers. Actually, $K^{km} = \sum_k \sum_m K^{km}$, $K^{AA} = \frac{1}{a}, K^{BB} = \frac{1}{1-a}, K^{AB} = K^{BA} = 0$. The same idea applies to L^{km}. The operators $(-\Delta)$ and $(-\Delta)^{-1}$ come from the inverse Fourier transform in the step to obtain (2.7). The main step involves the inversion of the relationship between the dependence of η_k on βU via the linearization around $\beta = 0$. $\bar{\eta}$ is the dominant term in the linearization. Integrating (2.7), we arrive at the following expression for $S(D_U)$:

$$-S(D_U) = \frac{1}{2\rho_0}\int_{R^3}[\frac{l^2K^{kk}}{6}|\nabla\eta_k|^2 + \frac{6L^{km}}{l^2N^2}((-\Delta)^{-1}(\eta_k - \bar{\eta}_k))(\eta_m - \bar{\eta}_m)]dx - S(D_0). \quad (2.8)$$

Then the approximate free energy (2.5) can be fully written as a functional of η,

$$\mathcal{F}(U) = \int_\Omega \frac{V^{km}}{2\rho_0}\eta_k\eta_m + \frac{l^2K^{kk}}{12\rho_0\beta}|\nabla\eta_k|^2 + \frac{3L^{km}}{l^2N^2\rho_0\beta}(-\Delta)^{-\frac{1}{2}}(\eta_k - \bar{\eta}_k)(-\Delta)^{-\frac{1}{2}}(\eta_m - \bar{\eta}_m)dx \quad (2.9)$$

We dropped the constant $S(D_0)$ and introduced the operator $(-\Delta)^{-\frac{1}{2}}$ in the above functional.

The last step in the derivation is to reduce the functional (2.9) to one scalar order parameter and rescale space in order to separate size effects of Ω from shape effects of Ω.

By setting

- $\chi = \beta V^{AB} - \frac{\beta(V^{AA}+V^{BB})}{2}$, which is a constant known as the Flory-Huggins parameter in polymer science,
- $D = \{x : |\Omega|^{\frac{1}{3}}x \in \Omega\}$,
- $\phi_A(x) = \frac{\eta_A(x)}{\rho_0}, \phi_B(x) = \frac{\eta_B(x)}{\rho_0}$, (one assumes that the diblock copolymer is incompressible in the sense $\phi_A(x) + \phi_B(x) = 1$)
- $u(x) = \phi_A(x) - \phi_B(x) = 1 - 2\phi_A(x), m = 1 - 2a$,
- $W(u) = \frac{1}{4}(1-u^2), \epsilon^2 = \frac{l^2}{3a(1-a)\chi|\Omega|^{\frac{2}{3}}}, \sigma = \frac{36|\Omega|^{\frac{2}{3}}}{a^2(1-a)^2l^2\chi N^2}$,

we finally arrive at

$$\mathcal{F}(u) = \frac{\epsilon^2}{2}\int_D |\nabla u|^2 dx + \int_D W(u)dx + \frac{\sigma}{2}\int_D |(-\Delta)^{-\frac{1}{2}}(u-m)|^2 dx,$$

which is the nonlocal Cahn-Hilliard energy functional.

2.4 Description of the Energy

From (2.1) we see that phase separation in diblock copolymer melts can be modeled by three main types of energy, namely the interfacial energy $\frac{\epsilon^2}{2}\int_D |\nabla u|^2 dx$, the double-well energy $\int_D W(u)dx$ and the nonlocal interaction energy $\frac{\sigma}{2}\int_D |(-\Delta)^{-\frac{1}{2}}(u-m)|^2 dx$. Actually, these three energies compete with each other in the process of phase separation. Here we describe each of these energies and discuss how the nonlocal term introduces additional competition with the Cahn-Hilliard portion of the energy. In this manner, we can get an intuitive feeling for what these terms like to minimize.

The Interfacial Energy: The interfacial energy acts much like the usual surface energy in two phase fluids. It penalizes rapid changes in monomer density u. Here, the parameter ϵ describes the amount of overlap between the two types of monomers, which is the interfacial thickness at the A and B monomer intersections, and is given by

$$\epsilon^2 = \frac{l^2}{3a(1-a)\chi|\Omega|^{\frac{2}{3}}} \tag{2.10}$$

It is easy to see that ϵ^2 is inversely proportional to the Flory-Huggins parameter χ. This interfacial energy concentrates along the transition regions between domains of A and B, and forces the configurations u to have as few transition regions as possible, in other words, it prefers large domains of a single monomer.

The Double-well Energy: $W(u)$ represents a double-well energy usually chosen to be $\frac{1}{4}(1-u^2)^2$, which prefers pure A and B phases ($u = \pm 1$) to a mixture. This term

penalizes the mixing of monomers, and would prefer a state whereby the system is segregated into pure A-rich and B-rich domains.

The Nonlocal Interaction Energy: This is the most interesting part of the energy. In the nonlocal term, the parameter σ is inversely proportional to N^2, and is given by

$$\sigma = \frac{36|\Omega|^{\frac{2}{3}}}{a^2(1-a)^2 l^2 \chi N^2}, \tag{2.11}$$

Δ is the Laplacian operator with Neumann boundary conditions. $(-\Delta)^{-\frac{1}{2}}$ is actually an integral operator. This nonlocal energy prefers to have a uniform density of value equal to the average density m, and penalizes densities whose local average are not equal to m.

Actually, the different subchains are all chemically bonded and the entropic penalty due to chain stretching is responsible for the nonlocal long-range interaction term, which is the third term. As we can easily see, when the energy functional is being minimized, the double-well energy $W(u)$ prefers to segregate monomers into pure A and pure B phases, and there is a competition between the interfacial energy term and the nonlocal term, assuming that u is close to 1 and -1 off the interface. The interfacial energy wants to minimize the area of interface. It prefers large domains of a single monomer. But the nonlocal term wants $u = m$. So if u takes the values of 1 or -1 in a large domain, the nonlocal energy does not become small. In order to make the third term small, u has to oscillate rapidly around m, which increases the area of interface.

2.5 Expected Minimizing Structures

In the last section, we talked about the role of each term in the free energy (2.1). Now arises the question: what do we expect to see for minimizers? Actually, structures of phase separation which are observed are highly periodic (Figure 1.1), like lamellar, spherical, cylindrical and gyroid, depending on the mean composition m. Let us take the two dimensional phase separation for example.

First of all, we consider the Cahn-Hilliard energy functional (2.2), where $\sigma = 0$. There are two cases, depending on the mean value m.

- $m = 0$: In this case, the length of the two subchains is equal. We expect to see two stripes in equal size. The interfacial surface separating the subdomains is a 'wall'.

- $m \neq 0$: In this case, the length of one subchain is greater than the other one. Two possible minimizing structures might be expected.

  1. Two subdomains, $A-$rich and $B-$rich, are separated by a 'wall', and one is bigger than the other one, shown in Figure 2.2 (a).
  2. Two subdomains are separated by a circle, shown in Figure 2.2 (b).

  The first case cannot happen, however, since the interfacial energy in the free energy functional prefers as small surface area as possible. Let us think about it in this way. Assume $m \to 1$(or -1), the subdomain of A (or B) will shrink. In the case shown in Figure 2.2 (a), the 'wall' should move in the direction which decreases the subdomain of A (or B), without any change in the area of the interfacial surface. In the case shown in Figure 2.2 (b), however, with the decreasing subdomain of A (or B), the perimeter of the circle is decreasing as well. Thus, circles are preferred for the nonzero mean values. The size of circles depends on the value of m.

Now, we move on to the nonlocal Cahn-Hilliard energy functional (2.1), where $\sigma \neq 0$. Heuristically, it is not hard to see that the nonlocal term prefers oscillation. Thus, we might expect to see periodic or nearly periodic patterns as the minimizing structures. We also consider the two cases.

- $m = 0$: Instead of the structure of two strips in the Cahn-Hilliard case, more alternating strips are anticipated as the value of σ increases (Figure 2.3 (a)).

- $m \neq 0$: Periodic circles (Figure 2.3 (b)).

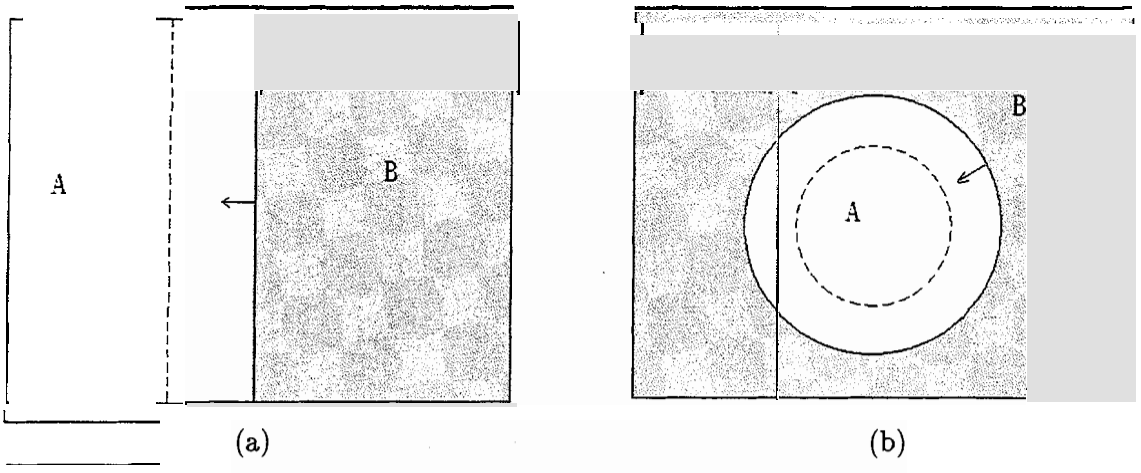

Figure 2.2: Two possible minimizing structures when $m \neq 0, \sigma = 0$. (a) The interfacial surface is a 'wall', which is rejected on physical grounds. (b) The interfacial surface is a circle, which is preferred.

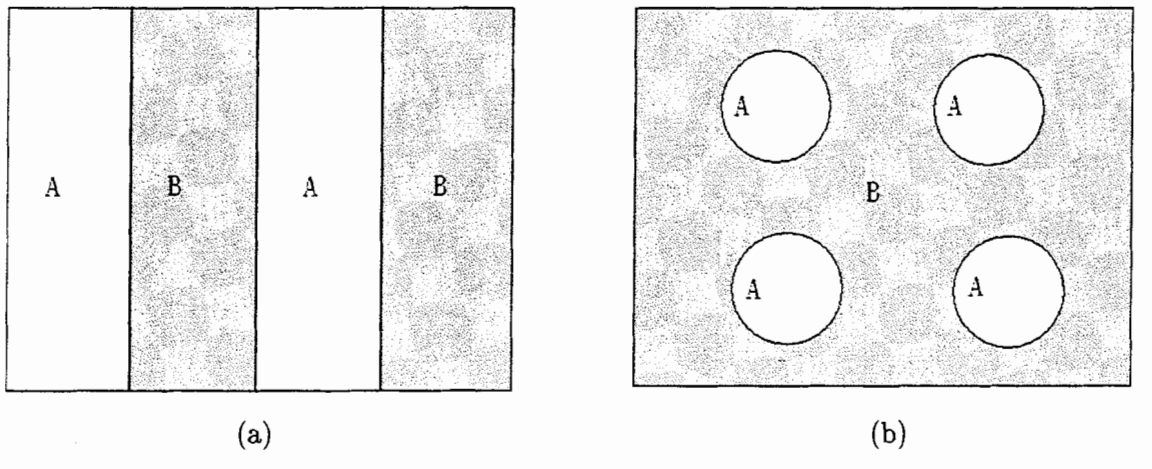

Figure 2.3: Expected minimizing structures when $\sigma \neq 0$. (a) Periodic strips for $m = 0$. (b) Periodic circles for $m \neq 0$.

In fact, ansatz-driven calculation ([16]), supplemented by rigorous analysis ([10]) through a scaling law suggests that periodicity scales like $(\frac{\epsilon}{\sigma})^{\frac{1}{3}}$. This argument strongly supports our expectations of periodic minimizing structures. In Chapter 5, we will see, these expected minimizing structures are well in accordance with our numerical results.

The nonlocal term not only prefers periodic structures on a small scale, but also influences the geometry of minimizers. Generally speaking, it is not always true that the phase boundaries of minimizers have constant mean curvature. It means that circles in two dimensional phase separation are not smooth. Recently, this observation was made by R. Choksi and P. Sternberg using a first variation calculation of a nonlocal isoperimetric problem [12]. Numerical experiments related to this issue remain our future work.

Chapter 3

Gradient Flows

3.1 The Basic Properties of a Gradient Flow

For a gradient flow, the basic idea is to start with an energy functional defined in a Hilbert space, and then write out the gradient flow associated with the functional and the Hilbert space, i.e.,

$$\frac{\partial u}{\partial t} = -K\text{grad}\mathcal{F}(u), \tag{3.1}$$

where K is some positive constant. From now on, we assume $K = 1$ for simplicity. This equation becomes an evolution equation which depends on the choice of Hilbert space. Whether it is a good model for the dynamics of the system is determined by the physical properties which the system should have.

As we mentioned earlier, a standard way of letting u evolve such that the free energy functional is decreasing in time is to let u evolve in the direction opposite to $\text{grad}\mathcal{F}(u)$. Actually, this evolution law guarantees that the free energy will not at least increase in time. If we assume u is a solution to (3.1), then we have

$$\frac{d}{dt}\mathcal{F}(u) = \langle \text{grad}\mathcal{F}(u), u_t\rangle_H = -K||\text{grad}\mathcal{F}(u)||_H^2 \leq 0, \tag{3.2}$$

under some chosen Hilbert space. $\langle\cdot,\cdot\rangle_H$ and $||\cdot||_H$ are the inner product and norm in the Hilbert space H, respectively. Therefore, $\mathcal{F}(u(t)) \leq \mathcal{F}(u(0))$ for all $t \geq 0$, which

means, the energy is not increasing in time. This property makes gradient flows of great importance for modeling physical problems.

3.2 Gradient Flow under L^2

As we see in (3.2), the inner product and norm are with respect to the chosen Hilbert space, and the choice of Hilbert space is crucial. Now let us try to write the gradient flow of the nonlocal Cahn-Hilliard energy functional under the $L^2(\Omega)$, which is the most obvious Hilbert space.

Recall that the constrained gradient operator grad$\mathcal{F}$ should satisfy the following equation:

$$\frac{d}{dt}\mathcal{F}(u+tv)|_{t=0} =< \text{grad}\mathcal{F}(u), v >_{L^2} . \tag{3.3}$$

for any smooth function $v(x)$. Now consider the nonlocal Cahn-Hilliard energy functional (2.1), we have,

$$\begin{aligned}
& \mathcal{F}(u+tv) - \mathcal{F}(u) \\
= & \int_D \frac{\epsilon^2}{2}|\nabla(u+tv)|^2 + W(u+tv) + \frac{\sigma}{2}|(-\Delta)^{-\frac{1}{2}}(u-m+tv)|^2 dx \\
& - \int_D \frac{\epsilon^2}{2}|\nabla u|^2 + W(u) + \frac{\sigma}{2}|(-\Delta)^{-\frac{1}{2}}(u-m)|^2 dx \\
= & \int_D \frac{\epsilon^2}{2}(|\nabla u|^2 + 2t\nabla u\cdot\nabla v + t^2|\nabla v|^2) - \frac{\epsilon^2}{2}|\nabla u|^2 dx \\
& + \int_D W(u+tv) - W(u) dx \\
& + \int_D \frac{\sigma}{2}|(-\Delta)^{-\frac{1}{2}}(u-m)|^2 + 2t(-\Delta)^{-\frac{1}{2}}(u-m)\cdot(-\Delta)^{-\frac{1}{2}}v + t^2|(-\Delta)^{-\frac{1}{2}}v|^2 \\
& \quad -\frac{\sigma}{2}|(-\Delta)^{-\frac{1}{2}}(u-m)|^2 dx \\
= & \int_D \frac{\epsilon^2}{2}(2t\nabla u\cdot\nabla v) + t^2|\nabla v|^2 dx + \int_D W(u+tv) - W(u) dx \\
& + \int_D \frac{\sigma}{2}(2t(-\Delta)^{-\frac{1}{2}}(u-m)\cdot(-\Delta)^{-\frac{1}{2}}v) + t^2|(-\Delta)^{-\frac{1}{2}}v|^2 dx
\end{aligned}$$

Then,

$$\begin{aligned}
\frac{d}{dt}\mathcal{F}(u+tv)|_{t=0} &= \lim_{t\to 0}\frac{\mathcal{F}(u+tv)-\mathcal{F}(u)}{t} \\
&= \int_D \epsilon^2\nabla u\cdot\nabla v dx + \lim_{t\to 0}\int_D \frac{W(u+tv)-W(u)}{t}dx \\
&\quad + \int_D \sigma(-\Delta)^{-\frac{1}{2}}(u-m)\cdot(-\Delta)^{-\frac{1}{2}}v)dx \\
&= \int_D \epsilon^2\nabla u\cdot\nabla v dx + \int_D W^{'}(u)vdx \\
&\quad + \int_D \sigma(-\Delta)^{-\frac{1}{2}}(u-m)\cdot(-\Delta)^{-\frac{1}{2}}v)dx.
\end{aligned}$$

Now using integration by parts and applying the boundary condition $\frac{\partial u}{\partial n}=0$, it follows that

$$\begin{aligned}
&= \int_D -\epsilon^2(\Delta u)vdx + \int_D W^{'}(u)vdx + \int_D \sigma(-\Delta)^{-1}(u-m)vdx \\
&= \int_D [-\epsilon^2\Delta u + W^{'}(u) + \sigma(-\Delta)^{-1}(u-m)]vdx \\
&= < -\epsilon^2\Delta u + W^{'}(u) + \sigma(-\Delta)^{-1}(u-m), v >_{L^2} .
\end{aligned}$$

Comparing this expression with equation (3.3), we arrive at the following equation:

$$\text{grad}\mathcal{F} = -\epsilon^2\Delta u + W^{'}(u) + \sigma(-\Delta)^{-1}(u-m),$$

it then follows that the evolution equation under L^2 is:

$$\frac{\partial u}{\partial t} = \epsilon^2\Delta u - W^{'}(u) - \sigma(-\Delta)^{-1}(u-m). \tag{3.4}$$

This equation is rejected, since it does not conserve mass in general. As we can see, using Green's First Identity and the boundary condition,

$$\begin{aligned}
\frac{d}{dt}\int_D u dx &= \int_D \epsilon^2\Delta u dx - \int_D W^{'}(u)dx - \int_D \sigma(-\Delta)^{-1}(u-m)dx \\
&= \int_{\partial D}\epsilon^2\frac{\partial u}{\partial n}dS - \int_D W^{'}(u)dx - \int_D \sigma(-\Delta)^{-1}(u-m)dx \\
&= -\int_D W^{'}(u) - \int_D \sigma(-\Delta)^{-1}(u-m)dx,
\end{aligned}$$

which is not always equal to zero. However, the conservation of mass can be guaranteed if we use a subspace of L^2 to write the gradient flow ([13]). The evolution equation under this subspace is

$$\frac{\partial u}{\partial t} = \epsilon^2 \Delta u - W'(u) + \sigma(-\Delta)^{-1}(u-m) + (W'(u))_D - \left(\sigma(-\Delta)^{-1}(u-m)\right)_D,$$

where $(\cdot)$ is the average over D. This equation is not used to model the process of phase separation because the extra terms are not local. Numerically, it is not convenient to solve compared with the one which is induced under $\dot{H}^{-1}$.

3.3 Gradient Flow under $\dot{H}^{-1}$

So far, we know L^2 space is rejected. Higher order Hilbert space $H^k, k > 0$, have the same difficulty. However, choosing the zero-average subspace of the dual of H^1 produces a more reasonable result, which is the modified Cahn-Hilliard equation, as we shall see in this section. For convenience, we denote this Hilbert space by $\dot{H}^{-1}$, which is different from H^{-1}.

Now let us see what kind of evolution equation is induced from this gradient flow under the Hilbert space $\dot{H}^{-1}$ ([13]).

Define

$$\dot{H}^{-1} := \{v : v = -\Delta f, f \in H^1, < v, 1 >_{L^2} = 0\}, \tag{3.5}$$

and the inner product in $\dot{H}^{-1}$

$$< v_1, v_2 >_{\dot{H}^{-1}} = < \nabla f_1, \nabla f_2 >_{L_2}, \tag{3.6}$$

where $v_1 = -\Delta f_1$ and $v_2 = -\Delta f_2$.

As pointed out already, the constrained gradient operator grad$\mathcal{F}$ should satisfy the following equation:

$$\frac{d}{dt}\mathcal{F}(u + tv)|_{t=0} = < \text{grad}\mathcal{F}(u), v >_{\dot{H}^{-1}} . \tag{3.7}$$

Now consider the function $v(x)$ satisfying

$$\int_D v(x)dx = 0, \tag{3.8}$$

and the boundary condition $\frac{\partial v}{\partial n} = 0$. Since (3.8) holds if and only if the homogeneous Neumann problem for

$$-\Delta f(x) = v(x) \tag{3.9}$$

has a unique solution $f(x)$ satisfying $\int f(x)dx = 0$. Using this expression for v and carrying out the same calculation as we did before, we can obtain

$$\begin{aligned}
\frac{d}{dt}\mathcal{F}(u+tv)|_{t=0} &= \int_D [-\epsilon^2\Delta u + W'(u) + \sigma(-\Delta)^{-1}(u-m)]v dx \\
&= -\int_D [-\epsilon^2\Delta u + W'(u) + \sigma(-\Delta)^{-1}(u-m)]\Delta f dx \\
&= -[-\epsilon^2\Delta u + W'(u) + \sigma(-\Delta)^{-1}(u-m)]\nabla f|_{\partial D} \\
&\quad + \int_D \nabla f \cdot \nabla[-\epsilon^2\Delta u + W'(u) + \sigma(-\Delta)^{-1}(u-m)]dx \\
&= < \nabla[-\epsilon^2\Delta u + W'(u) + \sigma(-\Delta)^{-1}(u-m)], \nabla f >_{L^2} . \qquad (3.10)
\end{aligned}$$

The boundary term is equal to zero because of the fact that the normal component of ∇f is zero. To apply the inner product under $\dot{H}^{-1}$ as defined above, we require that the first field have zero normal component on $\partial\Omega$, which is

$$\frac{\partial}{\partial n}(-\epsilon^2\Delta u + W'(u) - \sigma(-\Delta)^{-1}(u-m)) = 0. \tag{3.11}$$

Thus, we can obtain the inner product in $\dot{H}^{-1}$, which is

$$\begin{aligned}
&\frac{d}{dt}\mathcal{F}(u+tv)|_{t=0} \\
= \quad &< -\Delta[-\epsilon^2\Delta u + W'(u) - \sigma(-\Delta)^{-1}(u-m)], -\Delta f >_{\dot{H}^{-1}} \\
= \quad &< -\Delta[-\epsilon^2\Delta u + W'(u) - \sigma(-\Delta)^{-1}(u-m)], v >_{\dot{H}^{-1}} \qquad (3.12)
\end{aligned}$$

Now, take the equation (3.7) into consideration, we have the following equation,

$$< -\Delta[-\epsilon^2\Delta u + W'(u) - \sigma(-\Delta)^{-1}(u-m)], v >_{\dot{H}^{-1}} = < \text{grad}\mathcal{F}(u), v >_{\dot{H}^{-1}} . \tag{3.13}$$

Therefore, we identify

$$\text{grad}\mathcal{F}(u) = -\Delta[-\epsilon^2\Delta u + W'(u) - \sigma(-\Delta)^{-1}(u-m)]$$

The ansatz (3.1) now gives us the evolution law

$$\begin{aligned}
\frac{\partial u}{\partial t} &= \Delta[-\epsilon^2\Delta u + W'(u) - \sigma(-\Delta)^{-1}(u-m)] \\
&= \Delta[-\epsilon^2\Delta u + W'(u)] - \sigma(u-m). \qquad (3.14)
\end{aligned}$$

3.4 The Modified Cahn-Hilliard Equation

Based on the evolution equation (3.14) induced under $\dot{H}^{-1}$, we can introduce the modified Cahn-Hilliard equation. $W(u)$ is a double-well potential, normally given in the form $W(u) = \frac{1}{4}(1-u^2)^2$, $W'(u) = u^3 - u$. So from (3.14) we arrive at the following modified Cahn-Hilliard equation,

$$\frac{\partial u}{\partial t} = -\epsilon^2\Delta^2 u - \Delta u + \Delta u^3 - \sigma(u-m), \tag{3.15}$$

which is used in this thesis for numerical simulations. This modified equation conserves mass. Let us start with the mass conservative property of the Cahn-Hilliard equation, as we mentioned in the previous chapter.

$$\begin{aligned}
\frac{d}{dt}\int_D u dx &= \int_D -\epsilon^2\Delta^2 u dx + \int_D \Delta W'(u) dx \\
&= -\epsilon^2 \int_{\partial D} \frac{\partial(\Delta u)}{\partial n} dS + \int_{\partial D} \frac{\partial W'}{\partial n} dS \\
&= -\epsilon^2 \int_{\partial D} \frac{\partial(\Delta u)}{\partial n} dS + \int_{\partial D} W'' \frac{\partial u}{\partial n} dS \\
&= 0.
\end{aligned}$$

Boundary conditions are used in the last step.

As to the modified Cahn-Hilliard equation, we only need to consider the extra term $\sigma(u-m)$. Actually,

$$\int_D \sigma(u-m)dx = \sigma(\int_D u dx - \int_D m dx) = \sigma(\int_D u dx - m) = 0,$$

using (2.4), as well as the fact that D is a rescaled domain of Ω with volume 1.

Chapter 4

The Numerical Method

4.1 The Idea of the Split-Step Method

Consider a general evolution equation of the form

$$u_t = \mathcal{L}u + \mathcal{N}(u) \tag{4.1}$$

$$u(x,0) = u_0(x) \tag{4.2}$$

where $\mathcal{L}$ and $\mathcal{N}$ are linear and nonlinear operators, respectively. In general, the operators $\mathcal{L}$ and $\mathcal{N}$ do not commute (i.e., $\mathcal{L}\mathcal{N} \neq \mathcal{N}\mathcal{L}$) with each other. For instance, we have

$$\mathcal{L} = -\epsilon^2\Delta^2 - \Delta - \sigma \tag{4.3}$$

$$\mathcal{N}(u) = \Delta u^3 + \sigma m \tag{4.4}$$

for the nonlocal Cahn-Hilliard equation. The main idea in the split-step method is to approximate the exact solution of equation (4.1) by solving the purely linear and purely nonlinear equations in a given sequential order, in which the solution of one subproblem is employed as an initial condition for the next subproblem.

The solution of this equation may be advanced from one time-level to the next by means of the following formula

$$u(x,t+\Delta t) = e^{(\mathcal{L}+\mathcal{N}(u))\Delta t}u(x,t) + O((\Delta t)^2) \tag{4.5}$$

where Δt denotes the time step. In general, it is first order accurate in time. However, it turns out to be exact if operators $\mathcal{L}$ and $\mathcal{N}(u)$ are time-independent. In fact, by Taylor's theorem we have

$$u(x,t+\Delta t) = u(x,t) + u_t(x,t)\Delta t + \frac{1}{2!}u_{tt}(x,t)(\Delta t)^2 + ... \tag{4.6}$$

$$e^{\Delta t(\mathcal{L}+\mathcal{N}(u))}u(x,t) = u(x,t) + \Delta t(\mathcal{L}+\mathcal{N}(u))u(x,t) + \frac{1}{2!}(\Delta t)^2(\mathcal{L}+\mathcal{N}(u))^2u(x,t) + ... \tag{4.7}$$

Hence, equation (4.1) implies that (4.5) is first order accurate.

The time-splitting procedure now consists of replacing the right-hand side of (4.5) by an appropriate combination of products of the exponential operators $e^{\Delta t\mathcal{L}}$ and $e^{\Delta t\mathcal{N}(u)}$. An answer can be found by considering the Baker-Campbell-Hausdorff (BCH) formula for two operators A and B given by

$$e^{\lambda A}e^{\lambda B} = e^{\sum_{n=1}^{\infty}\lambda^n Z_n} \tag{4.8}$$

where $Z_1 = A + B$ and the remaining operators Z_n are commutators of A and B, commutators of commutators of A and B, etc., The expressions for Z_n are actually rather complicated, e.g.,

$$Z_2 = \frac{1}{2}[A,B]$$

where $[A,B] = AB - BA$ is the commutator of A and B, and

$$Z_3 = \frac{1}{12}([A,[A,B]] + [[A,B],B]).$$

From this result, one can easily get the first-order (known as Lie splitting) approximation of the exponential operator in (4.5) as follows

$$e^{\Delta t(\mathcal{L}+\mathcal{N}(u))} = e^{\Delta t\mathcal{L}}e^{\Delta t\mathcal{N}(u)} + O((\Delta t)^2). \tag{4.9}$$

Similarly, the second-order (known as Strang splitting) approximation

$$e^{\Delta t(\mathcal{L}+\mathcal{N}(u))} = e^{\frac{\Delta t}{2}\mathcal{L}}e^{\Delta t\mathcal{N}(u)}e^{\frac{\Delta t}{2}\mathcal{L}} + O((\Delta t)^3)$$

In this thesis, we consider the first-order splitting method.

It is convenient to view the scheme (4.9) as first solving the linear equation

$$u_t = \mathcal{L}u \tag{4.10}$$

then advancing the solution by solving the nonlinear equation

$$u_t = \mathcal{N}(u) \tag{4.11}$$

employing the solution of the former as the initial condition of the latter. Actually, we can see this in the following way. Define $u^n(x)$ to be the discrete approximation to the solution at time $t = n\Delta t$, and $v^n(x)$ to be the intermediate solution from solving the linear equation

$$v^n(x) = e^{\Delta t \mathcal{L}} u^n(x).$$

Then combining this equation and equation (4.9), we arrive at the approximate solution at time $t = (n+1)\Delta t$, using forward Euler method,

$$u^{n+1} = v^n + \Delta t \mathcal{N}(v^n).$$

That is, the advancement in time is carried out in two steps, the so called split-step method.

4.2 Spatial Discretization: Fourier method

Since we have periodic boundary conditions, it is possible to use a Fourier method, which has the advantage that the necessary discrete Fourier transform (DFT) operations can be computed efficiently using a fast Fourier transform (FFT).

4.2.1 The continuous Fourier transform

Suppose $f(x)$ is a complex-valued Lebesgue integrable function defined on $\mathcal{R}$. A Fourier transform to the domain of frequency, ω, is given by the function:

$$\hat{f}(\omega) = \int_{-\infty}^{\infty} f(x) e^{-i2\pi\omega x} dx \tag{4.12}$$

for every real number ω. The function (4.12) is called the Fourier transform of $f(x)$. We will refer to $\hat{f}(\omega)$ as being defined in the frequency domain and $f(x)$ as being defined in the spatial domain. The function $f(x)$ can be recovered from $\hat{f}(\omega)$ via the inverse Fourier transform, which is given by

$$f(x) = \int_{-\infty}^{\infty} \hat{f}(\omega) e^{i2\pi\omega x} d\omega. \tag{4.13}$$

Now, consider $f(x)$ as a continuous, L-periodic function defined on finite interval $[0, L]$, Then the Fourier transform and its inverse relations are, respectively:

$$\hat{f}(\omega) = \frac{1}{L} \int_0^L f(x) e^{-i\frac{2\pi\omega}{L}x} dx \tag{4.14}$$

and

$$f(x) = \sum_{\omega=-\infty}^{\infty} \hat{f}(\omega) e^{i\frac{2\pi\omega}{L}x}. \tag{4.15}$$

4.2.2 The discrete Fourier transform

Suppose the domain interval we use is $[0, 2\pi]$, application of the numerical method requires truncation of the infinite interval into a finite interval. The interval $[0, 2\pi]$ is divided into N equal subintervals with grid spacing $\Delta x = 2\pi/N$, where the integer N is chosen to be even. The spatial grid points are given by $x_j = 2\pi j/N, j = 0, 1, 2, ..., N$. The approximation solution to $u(x_j, t)$ is denoted by $U_j(t)$. The discrete Fourier transform of the sequence U_j, i.e.

$$\hat{U}_k = \mathcal{F}_k[U_j] = \frac{1}{N} \sum_{j=0}^{N-1} U_j e^{-ikx_j}, -\frac{N}{2} \leq k \leq \frac{N}{2} - 1 \tag{4.16}$$

gives the corresponding Fourier coefficients. Likewise, U_j can be recovered from the Fourier coefficients by the inverse of the discrete Fourier transform, as follows:

$$U_j = \mathcal{F}_j^{-1}[\hat{U}_k] = \sum_{k=-\frac{N}{2}}^{\frac{N}{2}-1} \hat{U}_k e^{ikx_j}, j = 0, 1, 2, ..., N-1, \tag{4.17}$$

where $\mathcal{F}$ denotes the discrete Fourier transform and $\mathcal{F}^{-1}$ its inverse. These transforms are efficiently computed using a fast Fourier transform (FFT) algorithm. Spatial derivatives of u may now be computed by first multiplying the Fourier coefficients, $\hat{U}_k$, by the power of ik corresponding to the order of the spatial derivative, and then applying the inverse Fourier transform. For example, the second order derivative u_{xx} at (x_j, t) is computed by $\mathcal{F}_j^{-1}[-k^2\mathcal{F}_k[U_j]]$ and the fourth order derivative u_{xxxx} is computed by $\mathcal{F}_j^{-1}[k^4\mathcal{F}_k[U_j]]$ and so on.

4.3 Time Integration

The nonlocal Cahn-Hilliard equation (NCH) is given by

$$u_t = -\epsilon^2\Delta^2 u - \Delta u + \Delta u^3 - \sigma(u - m). \tag{4.18}$$

As we have already mentioned, we consider a split-step method for the NCH equation, in which the linear equation is

$$u_t = (-\epsilon^2\Delta^2 - \Delta - \sigma)u \tag{4.19}$$

and the nonlinear equation is

$$u_t = \Delta u^3 + \sigma m. \tag{4.20}$$

These two equations are solved in a given sequential order(in our case, the linear equation is solved first) corresponding to the splitting formula given in Section 4.1.

From time t to the next time-level $t + \Delta t$, the solution of NCH equation may be advanced by the following two steps:

1. Advance the solution using only the linear equation:

$$u_t = \mathcal{L}u = (-\epsilon^2\Delta^2 - \Delta - \sigma)u \tag{4.21}$$

by means of the discrete Fourier transform and its inverse. In order to implement the time discretization we define u^n to be the discrete approximation to the solution $u(x,t)$ at $t = n\Delta t, n \leq M$. M is the number of time steps used. Then

equation (4.21) gives

$$v^n = e^{\Delta t \mathcal{L}} u^n. \tag{4.22}$$

To implement the spatial discretization using discrete Fourier transforms, we first replace u^{n+1} and u^n with their Fourier series. This gives

$$\hat{v}_k^n = e^{(-\epsilon^2 k^4 + k^2 - \sigma)\Delta t} \hat{u}_k^n, \quad k = -\infty, ..., \infty, \tag{4.23}$$

where $\hat{v}_k^n$ and $\hat{u}_k^n$ are the Fourier coefficient of the spatially continuous function v^n and u^n given by (4.14). We then replace $\hat{u}_k^n$ with its discrete equivalent $\hat{U}_k^n$ using $N-1$ points in space. Now equation (4.23) becomes

$$\hat{V}_k^n = e^{(-\epsilon^2 k^4 + k^2 - \sigma)\Delta t} \hat{U}_k^n, \quad k = -\frac{N}{2}, ..., \frac{N}{2} - 1. \tag{4.24}$$

Finally, we return the solution to the physical domain by applying the inverse discrete Fourier transform to (4.24). This step can be simply expressed as

$$V_j^n = \mathcal{F}^{-1}[e^{(-\epsilon^2 k^4 + k^2 - \sigma)\Delta t} \mathcal{F}_k[U_j^n]], \tag{4.25}$$

where U_j^n denotes the approximation to $u(x_j, n\Delta t)$.

2. Advance the solution according to the nonlinear part:

$$u_t = \mathcal{N}(u) = \Delta u^3 + \sigma m \tag{4.26}$$

using the solution obtained from the first step as the initial condition of this problem. The nonlinear term u^3 in equation (4.26) is handled pseudo-spectrally: as the solution in physical space evolves in time, the nonlinear term is computed at each time step by forming the power u^3 in physical space using the discrete value from the first step, and then applying the Fourier transform and applying the Laplacian in Fourier space. Finally transform back to physical space. Then the spatial discretization of the nonlinear partial differential equation (4.26) by a Fourier pseudo-spectal method can be written as

$$\dot{U}_j = \mathcal{F}^{-1}[-k^2 \mathcal{F}_k[(U_j)^3]] + \sigma m. \tag{4.27}$$

where the superposed dot means differentiation with respect to time. For the time integration of this equation, we use the forward Euler method. Then the idea of this step can be summarized as

$$U_j^{n+1} = V_j^n + \Delta t(\mathcal{F}^{-1}[-k^2\mathcal{F}_k[(V_j^n)^3]] + \sigma m). \tag{4.28}$$

From Section 4.1, we know the error in time from the splitting step is first order. Since the significant error in integrating from time t to time $t+\Delta t$ will be the temporal splitting error plus the temporal discretization error of the ordinary differential equations given by (4.27). As we know the forward Euler method is $O(\Delta t)$. Hence we say, the overall scheme is first order in time.

4.4 Test of the Laplacian in the Nonlinear Term

The nonlinear term in the Cahn-Hilliard equation is solved pseudo-spectrally as we discussed in the previous section. Since we do not want to magnify too much the error from spatial discretization, it is important to test the method of dealing with the Laplacian on the cubic term. The function we use for tests is the two dimensional function

$$f(x,y) = e^{\cos(3x)\sin(2y)}. \tag{4.29}$$

The exact value of Laplacian on f and f^3 are

$$\begin{aligned} \Delta f &= 9\sin(2y)e^{\cos(3x)\sin(2y)}[\sin^2(3x)\sin(2y) - \cos(3x)] \\ &\quad +4\cos(3x)e^{\cos(3x)\sin(2y)}[\cos^2(2y)\cos(3x) - \sin(2y)] \end{aligned} \tag{4.30}$$

$$\begin{aligned} \Delta f^3 &= 27\sin(2y)e^{3\cos(3x)\sin(2y)}[3\sin^2(3x)\sin(2y) - \cos(3x)] \\ &\quad +12\cos(3x)e^{3\cos(3x)\sin(2y)}[3\cos^2(2y)\cos(3x) - \sin(2y)], \end{aligned} \tag{4.31}$$

respectively.

As we can see from Figure 4.1, the errors decrease very rapidly until around 10^{-14}. Spectral accuracy is achieved when the nonlinear term is calculated pseudo-spectrally.

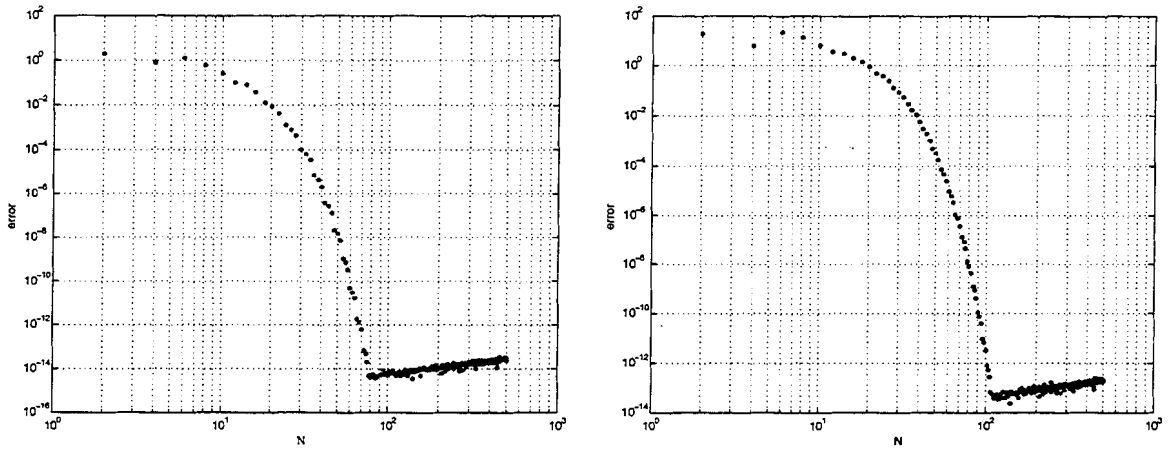

(a) Error of Δf (b) Error of Δf^3

Figure 4.1: Errors when Δf^3 is treated pseudo-spectrally for various N.

4.5 Stability Analysis

The problem of stability is pervasive in the numerical solution of partial differential equations. Since our scheme is composed of two partial differential equations, the stability of each part is sufficient to show that of the overall scheme.

As we know, given a time dependent problem, firstly it is discretized with respect to space, which generates a system of ordinary differential equations. Then the system of ordinary differential equations is solved by a finite difference method in time. In order to investigate the eigenvalue stability of this process, we should consider the following question: *under what conditions are the eigenvalues of the spectral differentiation operator contained in the stability region of the time discretization formula?*

In the first step of the process of solving the Cahn-Hilliard equation, a linear time dependent equation is solved in Fourier space, which is,

$$\hat{V}_k^n = e^{(-\epsilon^2 k^4 + k^2 - \sigma)\Delta t} \hat{U}_k^n. \tag{4.32}$$

In fact equation (4.32) gives us the amplification factor

$$A(k) = e^{(-\epsilon^2 k^4 + k^2 - \sigma)\Delta t}. \tag{4.33}$$

According to Von Neumann condition, the formula as described is stable if the amplification factor satisfies $|A(k)| \leq 1$. This indicates,

$$\begin{aligned} |A(k)| = |e^{(-\epsilon^2 k^4 + k^2 - \sigma)\Delta t}| &\leq 1 \\ (-\epsilon^2 k^4 + k^2 - \sigma)\Delta t &\leq 0 \\ \epsilon^2 k^4 - k^2 + \sigma &\geq 0. \end{aligned} \tag{4.34}$$

The last inequality gives us a restriction on the parameters ϵ, σ and the wavelength k, not on Δt. Therefore, this step only, as long as (4.34) holds, is stable with any choice of time step Δt. This condition determines the stability of $u = 0$ under small perturbations. The modes k such that (4.34) is not satisfied will grow leading to pattern formation.

Now let us switch to the second step, solving the nonlinear equation. The forward Euler method is used in time to deal with the system of ordinary differential equations. The stable region for forward Euler method is shown in Figure 4.2, which was obtained using the recurrence relation ([25]). Then the problem becomes to determine the eigenvalues of the spectral differentiation matrix. First, we quote a theorem by Trefethen ([25]).

Theorem 1. *For a periodic problem with spatial domain* $[0, 2\pi)$*, suppose the grid points* N *is even, and* m *denotes the order of spatial differentiation.*

If m *is odd, the* m*th-order spectral differentiation matrix* $D^{(m)}$ *is a skew-symmetric matrix with eigenvalues* $[-i(\frac{\pi}{\Delta x} - 1)^m, i(\frac{\pi}{\Delta x} - 1)^m]$*, and norm*

$$||D^{(m)}|| = \left(\frac{\pi}{\Delta x}\right)^m.$$

If m *is even,* $D^{(m)}$ *is a symmetric matrix with eigenvalues* $(-1)^{\frac{m}{2}} \times [0, (\frac{\pi}{\Delta x})^m]$*, and norm*

$$||D^{(m)}|| = \left(\frac{\pi}{\Delta x}\right)^m. \tag{4.35}$$

Applying this theorem to our equation $u_t = \Delta u^3 + \sigma m$, whose spectral differentiation matrix is $D_N^{(2)}$, the eigenvalues are all real and given by $[-(\frac{\pi}{\Delta x})^2, 0]$. Take into

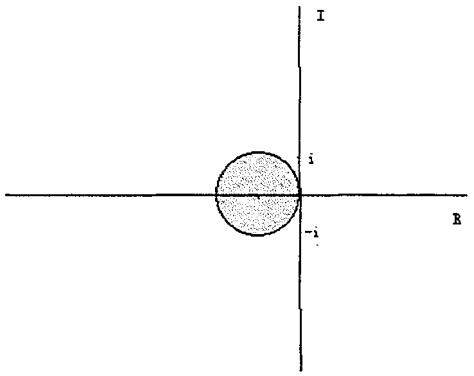

Figure 4.2: The stable region for forward Euler method, which is a circle centered at (-1, 0) with radius 1.

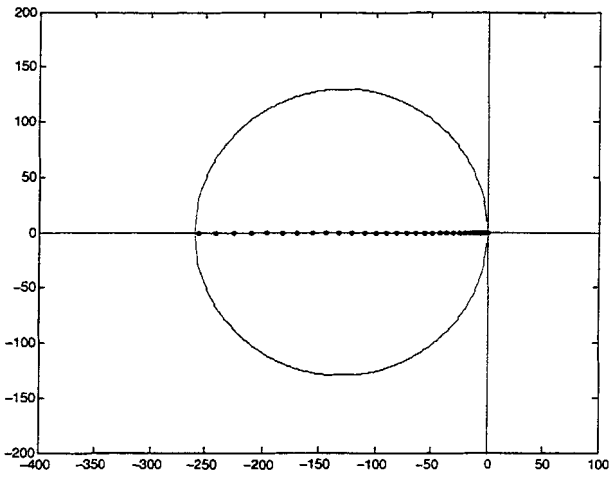

Figure 4.3: Eigenvalues of $D_N^{(2)}$, superimposed on the stable region for forward Euler method, for $N = 32$.

consideration the stability restriction, all these eigenvalues should lie in the circle. In this case, it should be the real axis within the circle in Figure 4.2. Hence, we arrive at the following stability condition,

$$\left(\frac{\pi}{\Delta x}\right)^2 \leq \frac{2}{\Delta t}, \tag{4.36}$$

which is equivalent to

$$\Delta t \leq \left(\frac{2}{\pi^2}\right)(\Delta x)^2. \tag{4.37}$$

Figure 4.3 shows the eigenvalues of $D_N^{(2)}$ when $N = 32$. They are within the stable region for forward Euler method. In conclusion, in order to keep our method stable,

$$\epsilon^2 k^4 - k^2 + \sigma \geq 0, \text{and}, \Delta t \leq \left(\frac{2}{\pi^2}\right)(\Delta x)^2 \tag{4.38}$$

should both be guaranteed.

Chapter 5

Numerical Results

An initially homogeneous disordered phase separates into ordered structures when the temperature is quenched below a critical value. The modified Cahn-Hilliard equation models this process. As we know, the parameter σ is inversely proportional to the square of the total chain length N of the copolymer. The number N is in general quite large, hence σ is very small. ϵ represents the interfacial thickness at the bonding point assumed to be sufficiently small. In the numerical experiments, we do not want ϵ to be either too small or too large, otherwise, the property of phase separation can not be well captured. So we should choose a suitable value for ϵ ($\epsilon = 0.08$ is a good one for numerical tests). The average $m \in [-1, 1]$ stands for the ratio of components of two homopolymers.

Depending on the ratio of two subchains of diblock copolymer (i.e., m), there appears a variety of morphologies for the asymptotic steady states of the modified Cahn-Hilliard equation (3.15). For instance, it is confirmed experimentally that a double-diamond structure appears near $m = 0$ besides lamellar and cylindrical structure, and many other types of morphologies could be discovered even for the same values of m. This suggests the coexistence of multiple stable steady states, although the basin of attraction of each morphology changes depending on m. From previous discussions, we know from the competition of the three parts in the free energy, there is a possibility that the free energy may have local minimizers which correspond to metastable states of the physical

system.

We take as initial condition a random perturbation of a uniform mixture as follows:

$$u(x,0) = m + Cr(x), \tag{5.1}$$

where the random variable $r(x)$ is uniformly distributed in $[-1,1]$ and has zero mean ([17]). m is the constant concentration of the uniform mixture. C is taken as 0.05 throughout our experiments. The domain is $[0,2\pi]^n$, where $n = 1,2$ or 3 is the space dimension.

5.1 Conservation Property

One important property of Cahn-Hilliard system is its mass conservation,

$$I = \int_D u dx = m. \tag{5.2}$$

To examine the conservation property of the split-step scheme, we calculate the discrete analogue of the conserved quantity I. The relative error denoted by δ is defined by

$$\delta = \frac{|\bar{I} - \bar{I}_t|}{|\bar{I}_t|}, \tag{5.3}$$

where $\bar{I}$ and $\bar{I}_t$ represent the calculated values of the conserved quantity I at initial time and terminating time. The trapezoidal rule is used for the numerical quadrature of the integral.

Dim	$\delta\|_{m=0}$	$\delta\|_{m=0.4}$	$\delta\|_{m=0.5}$	time
1D	1.3696E-15	2.9747E-13	5.0535E-15	800
2D	3.3217E-13	2.4923E-14	8.7873E-15	1000
3D	3.8605E-13	4.9577E-14	6.1943E-14	1000

Table 5.1: The conservation error δ of three different mean values, in one, two and three-space dimensional cases. $\epsilon = 0.08, \sigma = 0$.

The relative errors δ are given in Table 5.1. We consider one, two and as well as three spatial dimensions, with mean values $m = 0$, $m = 0.4$ and $m = 0.5$. The terminating time is chosen to make sure that the final state is stable. σ is set to be zero in all these cases, so the nonlocal term is excluded. The results show that the conserved quantity is extremely well preserved for the split-step scheme. As to the case where σ is not zero, the same conclusion can be drawn.

5.2 One Dimensional Phase Separation

One dimensional phase separation is not physically realistic. But with no doubt it gives us a basic idea on what the minimizers look like and how the order parameter evolves with time. And as well we can more or less extrapolate the minimizing structures in two dimensional separation, but not the three dimensional separation because of the complexity of the patterns.

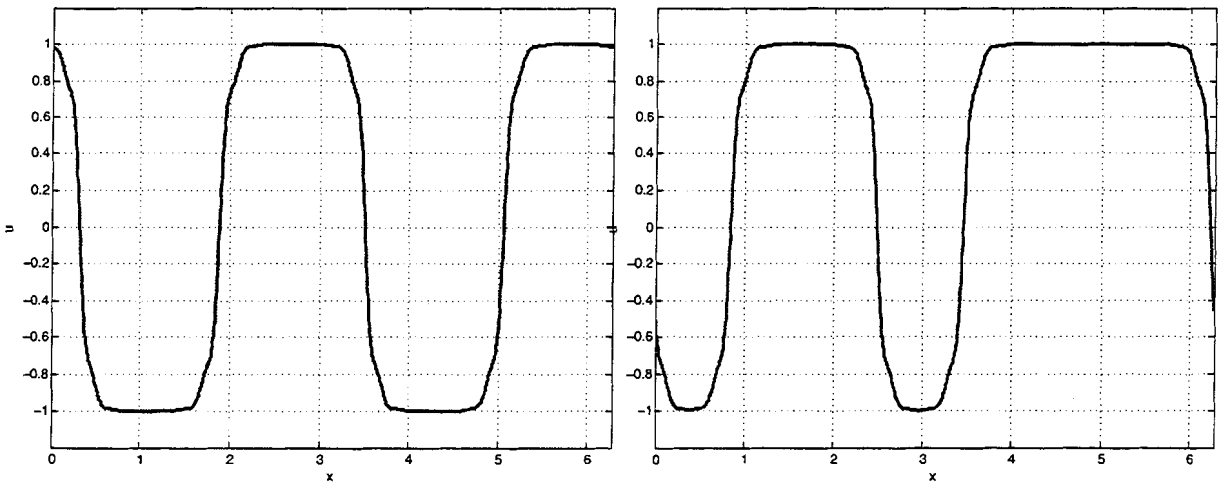

(a) m=0 (b) m=0.4

Figure 5.1: Metastable states of u with mean values $m = 0$ and $m = 0.4$, respectively. $N = 1024, \sigma = 0, \epsilon = 0.08$.

We know m denotes the mean value of the order parameter. As might be expected,

the final stable state should be given by alternating values of 1 and -1. As a simple illustration, consider a symmetric diblock copolymer melt with $m = 0$, which means the two subchains are of equal length. The domain size of $u = 1$ and $u = -1$ should be the same. Whereas if $m \neq 0$, say, $m = 0.4$, the domain size of $u = 1$ should be greater than that of $u = -1$. Figure 5.1 shows metastable structures of these two cases. In this example, we consider a spatial mesh of 1024 points, $\sigma = 0$ and $\epsilon = 0.08$. The results with σ nonzero are shown in Figure 5.2. Take into consideration of the role of the nonlocal energy in nonlocal Cahn-Hilliard functional, we know, the bigger the σ is, the more oscillations we will see.

5.3 Two Dimensional Phase Separation

The resolution we use for 2D phase separation is 64×64 or 128×128. In our first example we consider $\sigma = 0$ which is the Cahn-Hilliard case, and $m = 0$ which corresponds to the case of equal sized subchains A and B.

Figure 5.3 shows snapshots of the solution plotted as filled contours with mean value $m = 0$. The lightest phase corresponds to $u = 1$ and the darkest one to $u = -1$. The homogeneous mixture undergoes a fast separation followed by a slow coarsening procedure. This figure together with Figure 5.4 exhibit the minimizing structure which shows nice stripes. This result agrees with our expectation. Evolution of u with mean value $m = 0.4$ is shown in Figure 5.6. Figure 5.5 and Figure 5.7 are the cases where σ is nonzero.

5.3.1 The role of m

Different ratios of the two subchains give different stable patterns. From the results we obtained in one dimensional separation, we may conjecture, in two dimensional phase separation, equal-sized strips for $m = 0$, and unequal-sized ones for $m \neq 0$. However, when $m \neq 0$, as we discussed in Chapter 2, circles are much more preferred than strips because they have lower energy. In two dimensional separation, there are normally two

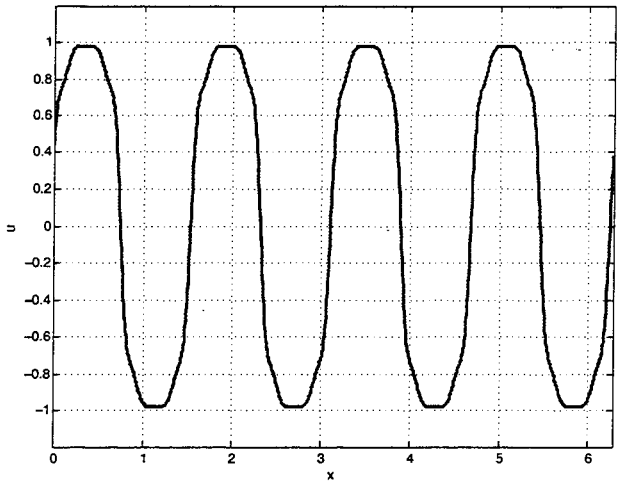

(a) $\sigma = 0.1$

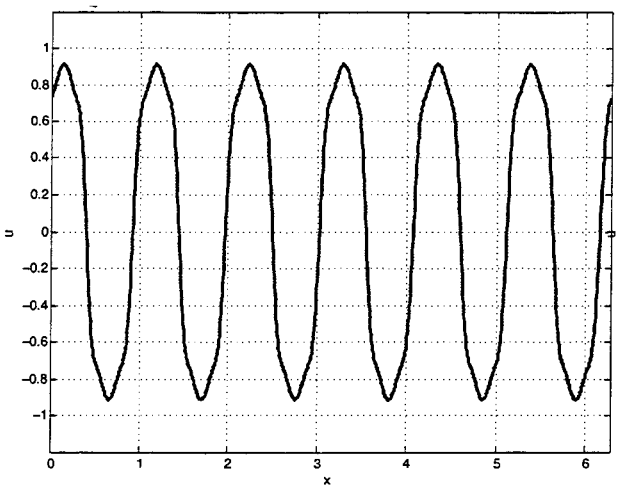

(b) $\sigma = 0.8$

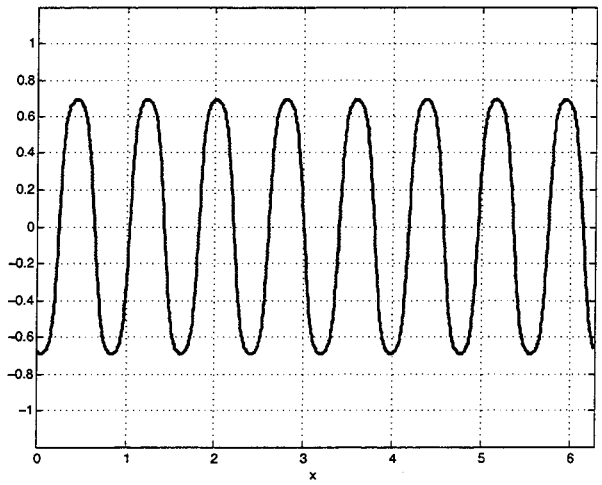

(c) $\sigma = 6.4$

Figure 5.2: Stable state of u with mean value $m = 0$ but different values of σ: $(a)\sigma = 0.1, (b)\sigma = 0.8, (c)\sigma = 6.4.N = 1024, \epsilon = 0.08$.

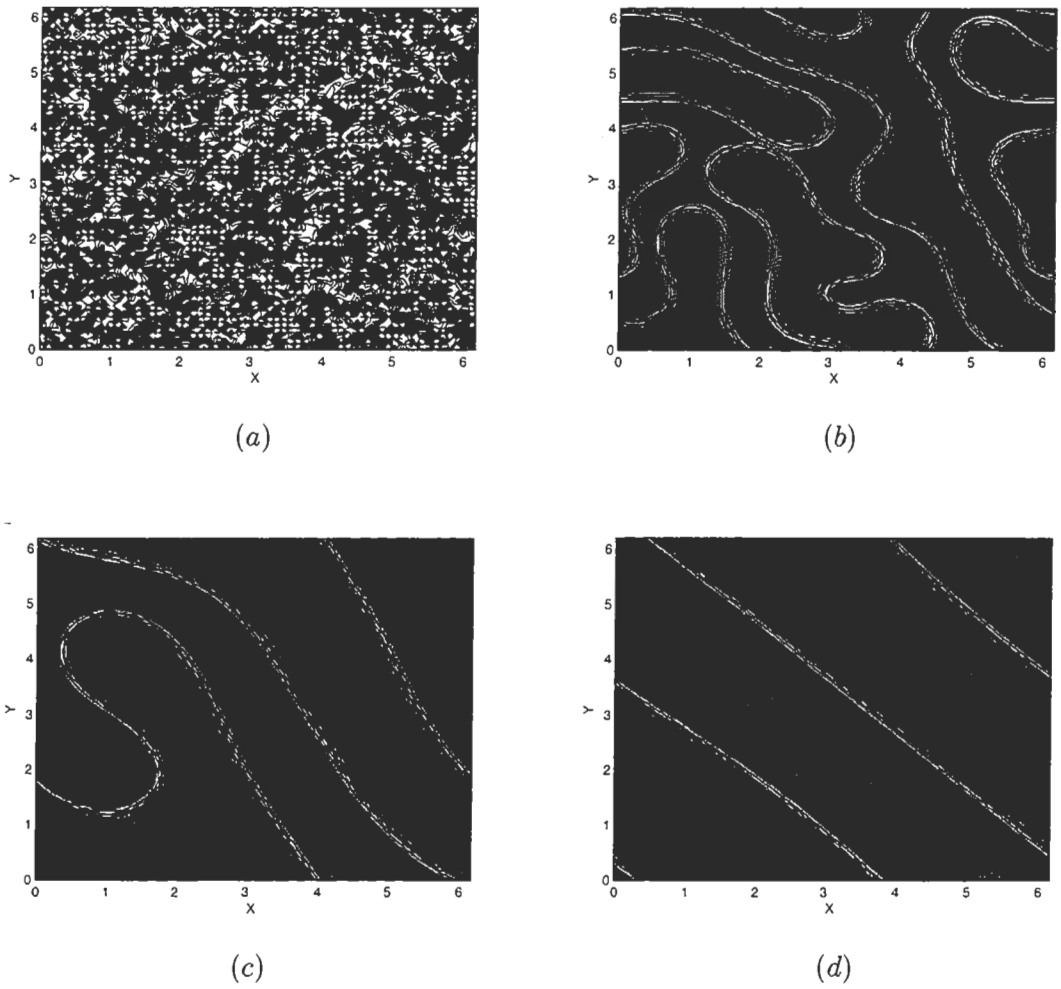

Figure 5.3: Evolution of u with mean value $m = 0$, represented in filled contours, at different time: $(a)t = 0.0019, (b)t = 5.78, (c)t = 48.25, (d)t = 386$. $N = 64, \sigma = 0, \epsilon = 0.08, \Delta t = 0.0019$. The lightest phase corresponds to $u = 1$ and the darkest phase corresponds to $u = -1$. Figure (d) shows a metastable state of $m = 0$.

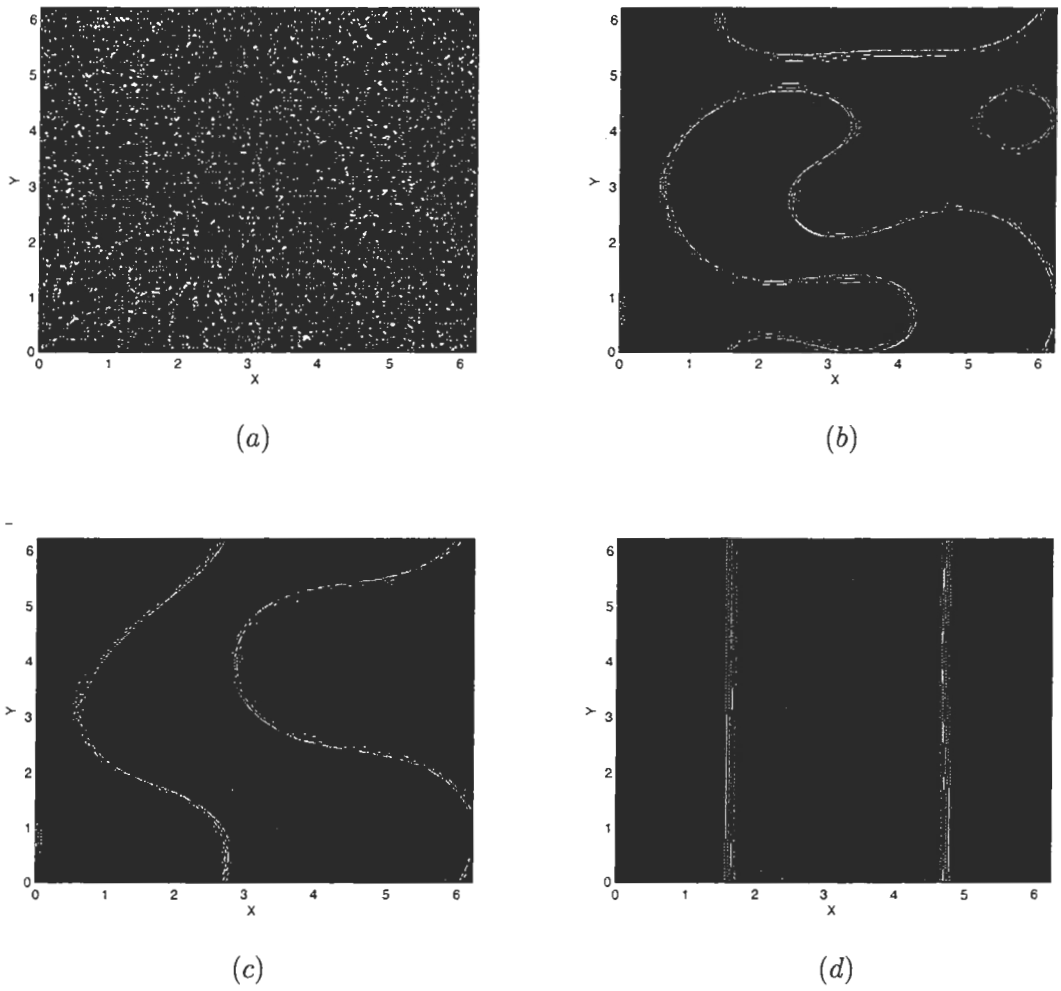

Figure 5.4: Evolution of u with mean value $m = 0$, represented in filled contours, at different time: $(a)t = 0.00024, (b)t = 14.4, (c)t = 28.8, (d)t = 156$. $N = 128, \sigma = 0, \epsilon = 0.08, \Delta t = 0.00024$. The lightest phase corresponds to $u = 1$ and the darkest phase corresponds to $u = -1$. Figure (d) shows the stable state of $m = 0$.

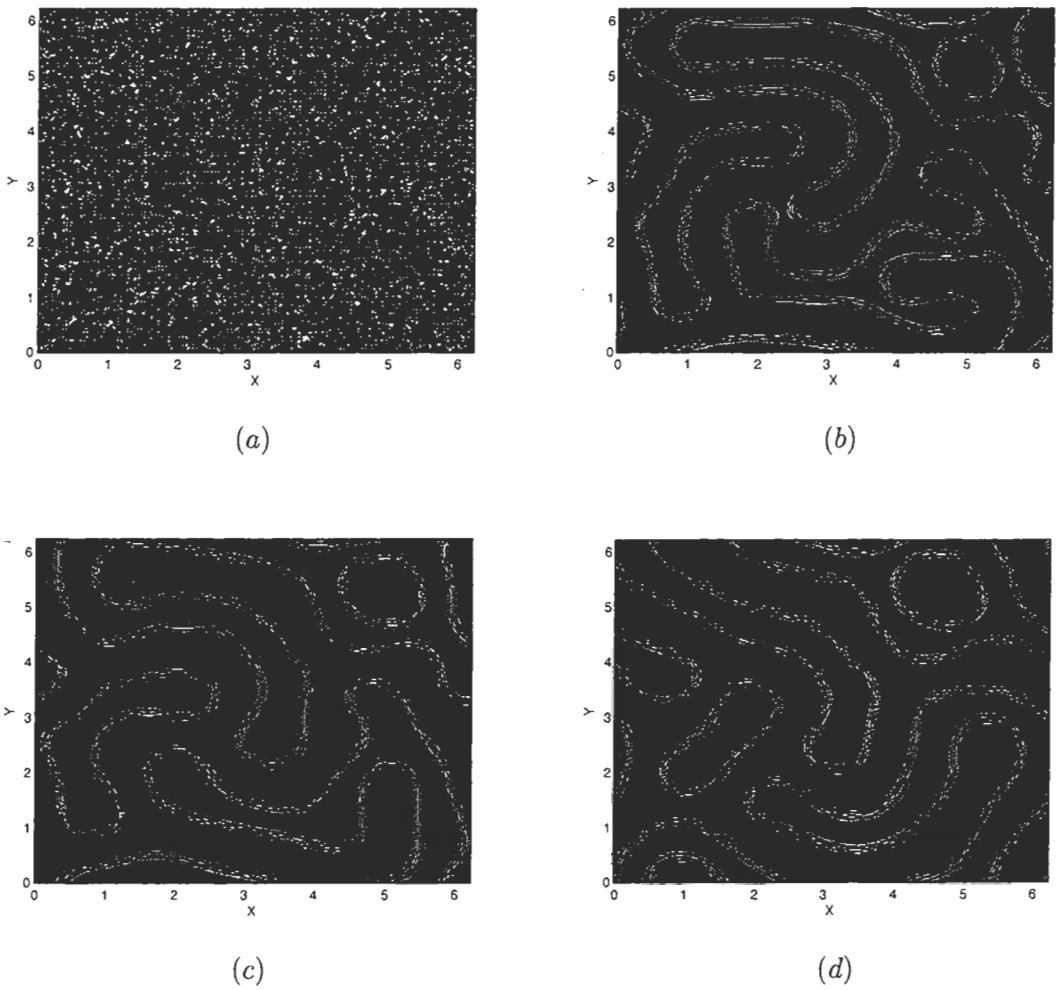

Figure 5.5: Evolution of u with mean value $m = 0$, represented in flooded contours, at different time: $(a)t = 0.00024, (b)t = 2.39, (c)t = 23.93, (d)t = 203.42$. $N = 128, \sigma = 3.2, \epsilon = 0.08, \Delta t = 0.00024$. Figure (d) shows a metastable state of $m = 0$ and $\sigma = 3.2$. Since σ is not equal to zero, more than two strips are expected to see as the stable state, which can be obtained if we add some noises on this metastable state.

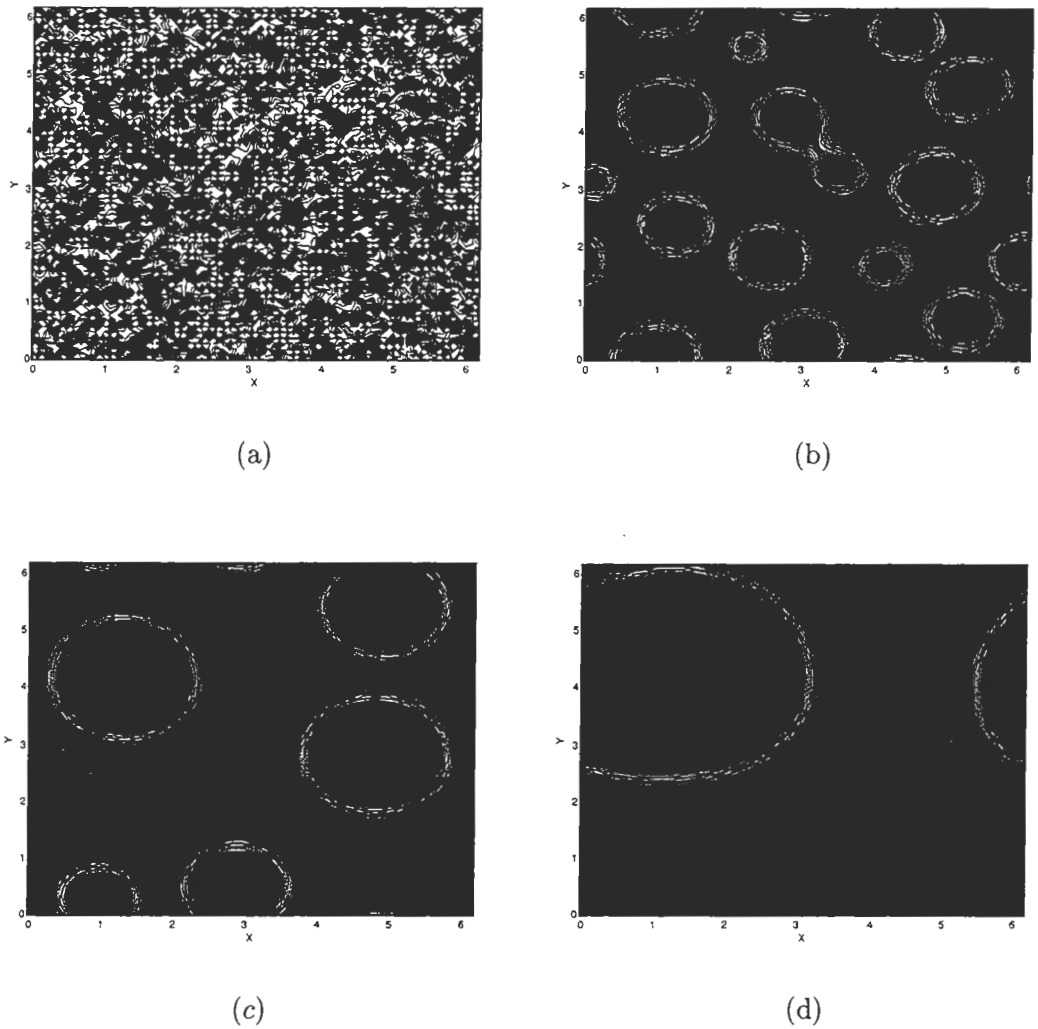

Figure 5.6: Evolution of u with mean value $m = 0.4$, represented in flooded contours, at different time: $(a)t = 0.0019, (b)t = 7.71, (c)t = 92.53, (d)t = 443.9$. $N = 64, \sigma = 0, \epsilon = 0.08, \Delta t = 0.0019$. The phases enclosed by circles correspond to $u = -1$ and the phases outside circles correspond to $u = 1$. One circle with periodic boundary condition is shown in Figure (d) as the stable state.

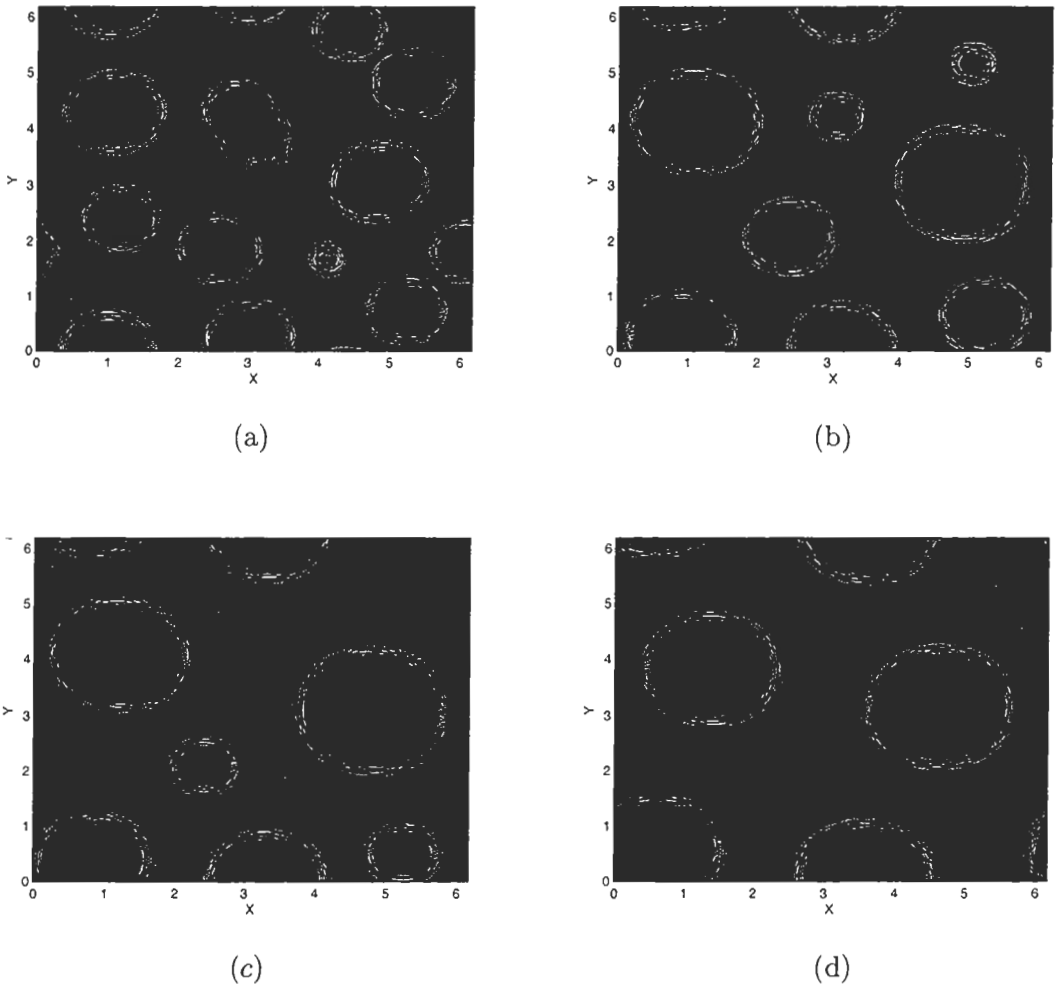

(a) (b)

(c) (d)

Figure 5.7: Evolution of u with mean value $m = 0.4$, represented in flooded contours, at different time: $(a)t = 9.62, (b)t = 65.38, (c)t = 90.38, (d)t = 192.31$. $N = 64, \sigma = 0.1, \epsilon = 0.08, \Delta t = 0.0019$. The phases enclosed by circles correspond to $u = -1$ and the phases outside circles correspond to $u = 1$. In Figure (d), which shows the stable state of $m = 0.4, \sigma = 0.1$, all circles are uniform.

kinds of globally stable state. One is the lamellar structure with $m = 0$, shown in Figure 5.3, and the other is the circle pattern shown in Figure 5.6, whose mean value $m \neq 0$. Note that because of the competition of those three energy terms, metastable states do exist.

5.3.2 The role of σ

In this section, we consider the role of σ. The role of σ plays is clearly shown here: the nonlocal term prefers oscillation between domains of each monomer. In other words, as the value of σ increases, we should see finer structures. Now let us examine carefully the relationship of σ and the periodicity. It has been shown that the domain width or periodicity scales like $(\frac{\epsilon}{\sigma})^{\frac{1}{3}}$(see [10] and the references therein). Then, roughly speaking, if we want to double the periodicity (when the mophology is stable, i.e., lamellar, cylindrical, spherical), we should have,

$$(\frac{\epsilon_1}{\sigma_1})^{\frac{1}{3}} \sim 2(\frac{\epsilon_2}{\sigma_2})^{\frac{1}{3}}$$
$$8\epsilon_2\sigma_1 \sim \epsilon_1\sigma_2.$$

This indicates a relationship of the value of σ, ϵ and the periodicity.

Figure 5.8 shows the stable patterns with an increasing σ. In each of these cases, random initial condition is chosen, and the volume fraction is $m = 0.4$, which implies the 'round' case, as shown in the figures. The stable states shown here are well assembled periodic structures.

Now let us consider another case in which a different initial condition is adopted to see the role of σ. Suppose the domain considered is $L \times L$. And

$$\begin{cases} u = -1, & \text{if } x \leq \frac{L}{2}, y \in [0, L] \\ u = 1, & \text{if } x > \frac{L}{2}, y \in [0, L] \end{cases} \tag{5.4}$$

is set to be the initial condition instead of the random condition, which is mostly used for our numerical simulations. Actually, the domain is divided into two equal parts by setting one part equal to -1 and the other part 1. By this preposed condition, one side

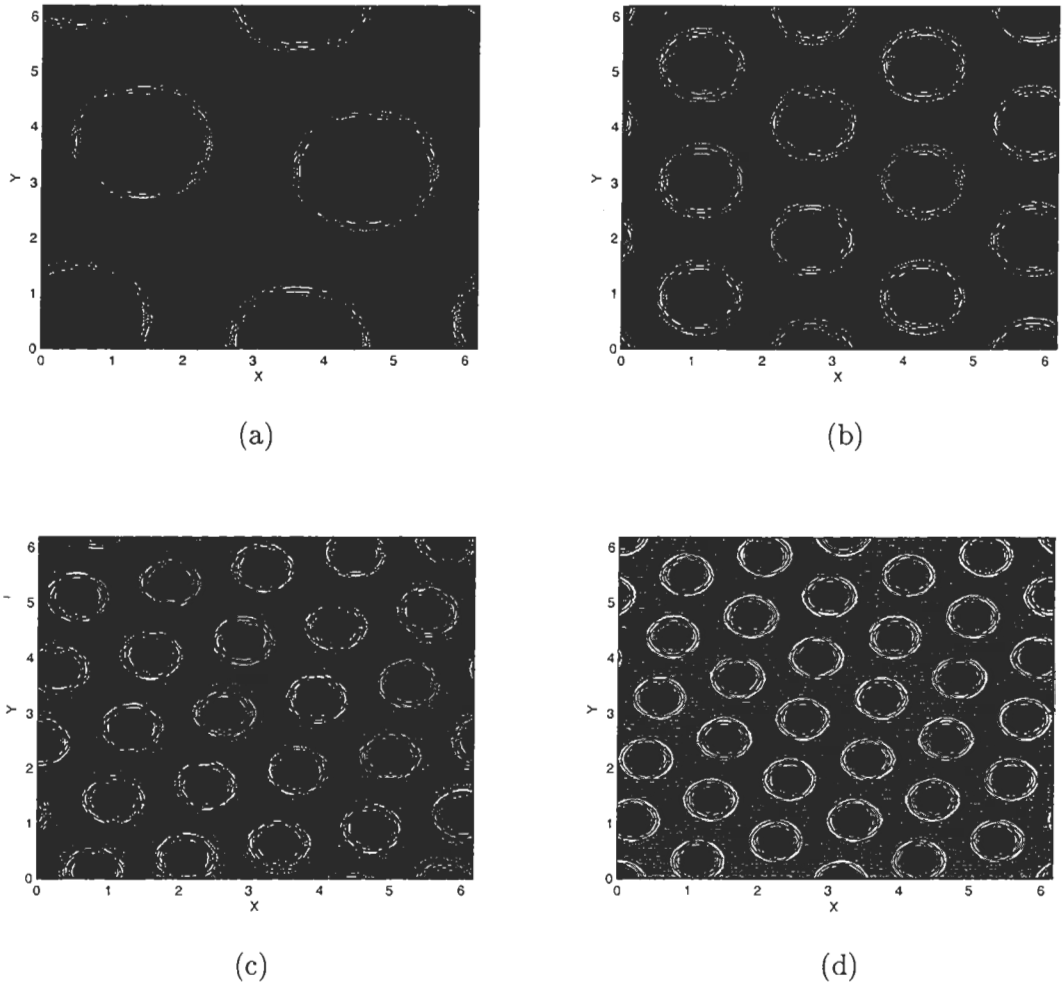

Figure 5.8: Stable state of u with mean value $m = 0.4$ but different σ: $(a)\sigma = 0.1, (b)\sigma = 0.8, (c)\sigma = 3.2, (d)\sigma = 6.4$. $N = 64, \epsilon = 0.08, \Delta t = 0.0019$. The phases enclosed by circles correspond to $u = -1$ and the phases outside circles correspond to $u = 1$. From these figures we can tell the larger the σ is, the smaller the periodicity is.

is all A (or B) monomers, and the other one is all B (or A) monomers. Figure 5.9 (a) shows this kind of initial condition. In fact it is also the stable state of the Cahn-Hilliard equation ($\sigma = 0$), since the two types of monomers are already fully separated at the very beginning. With increasing σ, more strips with same width (mean value $m = 0$) are generated.

5.4 Three Dimensional Phase Separation

We now turn to three dimensional simulations of phase separation. First we take the mean value $m = 0$ and $\sigma = 0$ and render the isosurface of separation of the two types of monomers at $u = 0$. Figure 5.10 gives representative snapshots of the isosurface of separation. Notice that the complexity of the patterns cannot be extrapolated from the one dimensional or two dimensional counterparts.

Figure 5.11 and Figure 5.12 present the two stages of the phase separation. The first stage is a fast separation process during which the formation of the phases can be observed. And the second one is a stage of coarsening which takes much longer. During the first stage, Figure 5.11, the uniform structure becomes a fine-grained mixture of two different phases, each of which corresponds to a stable concentration configuration. This stage usually takes a relatively short time. When the phase regions are formed, the evolution of the concentration enters the second stage, phase coarsening, during which the configuration of phase regions is coarsened, the originally fine-grained structure becomes enlarged, and the geometric shape of the phase regions become simpler and simpler, finally tending to regions of minimum surface area.

5.4.1 The role of m

As mentioned by Ohta and Kawasaaki [16], the earlier work done by Kampf et al. for the system polystyrene-polybutadiene(S-B) plus styrene, the following structure is reported: $0 - 25\%$ S for S spheres in a B matrix, $25 - 40\%$ S for an S cylinder in a B matrix, $40 - 60\%$ S for lamellar structures, $60 - 85\%$ S for a B cylinder in an S matrix, and

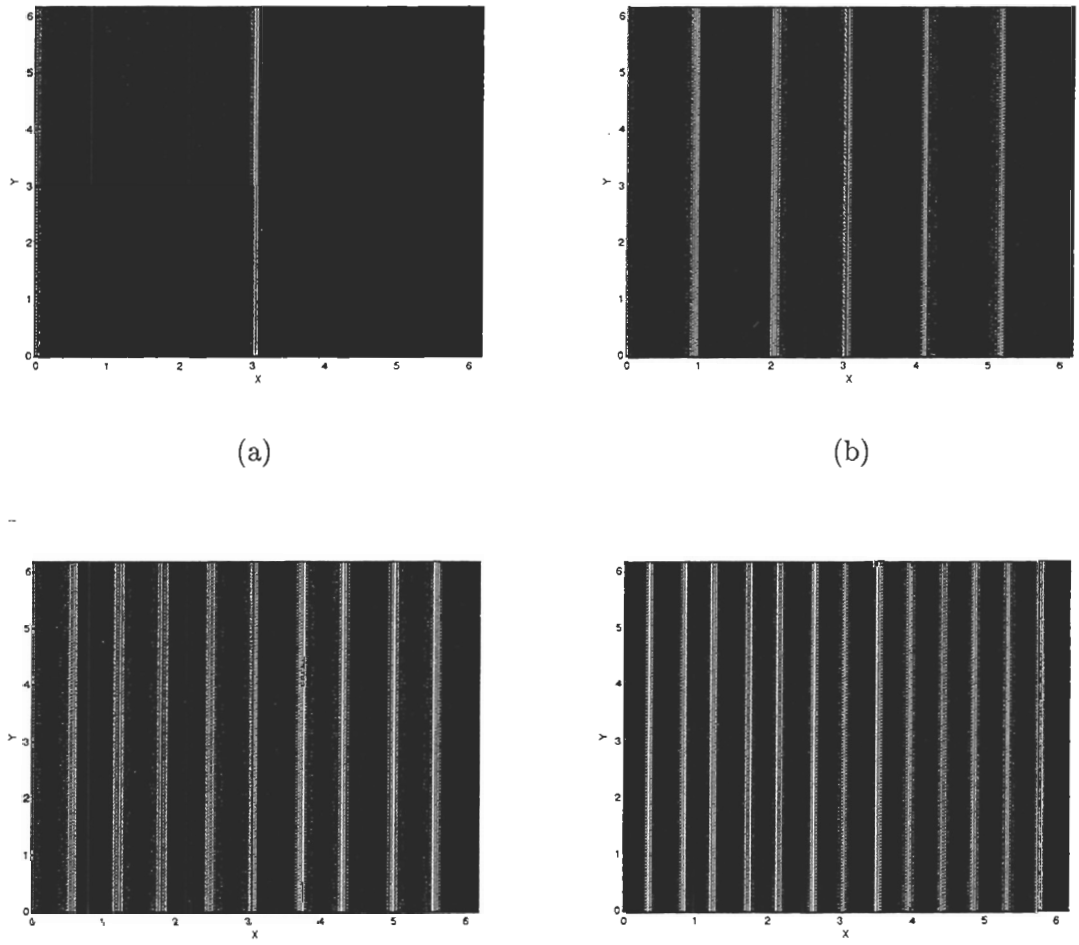

Figure 5.9: Stable state of u with mean value $m = 0$ but different σ: $(a)\sigma = 0, (b)\sigma = 0.8, (c)\sigma = 3.2, (d)\sigma = 6.4$. Equation (5.4) is used as the initial condition. $N = 64, m = 0, \epsilon = 0.08, \Delta t = 0.0019, T = 200$.

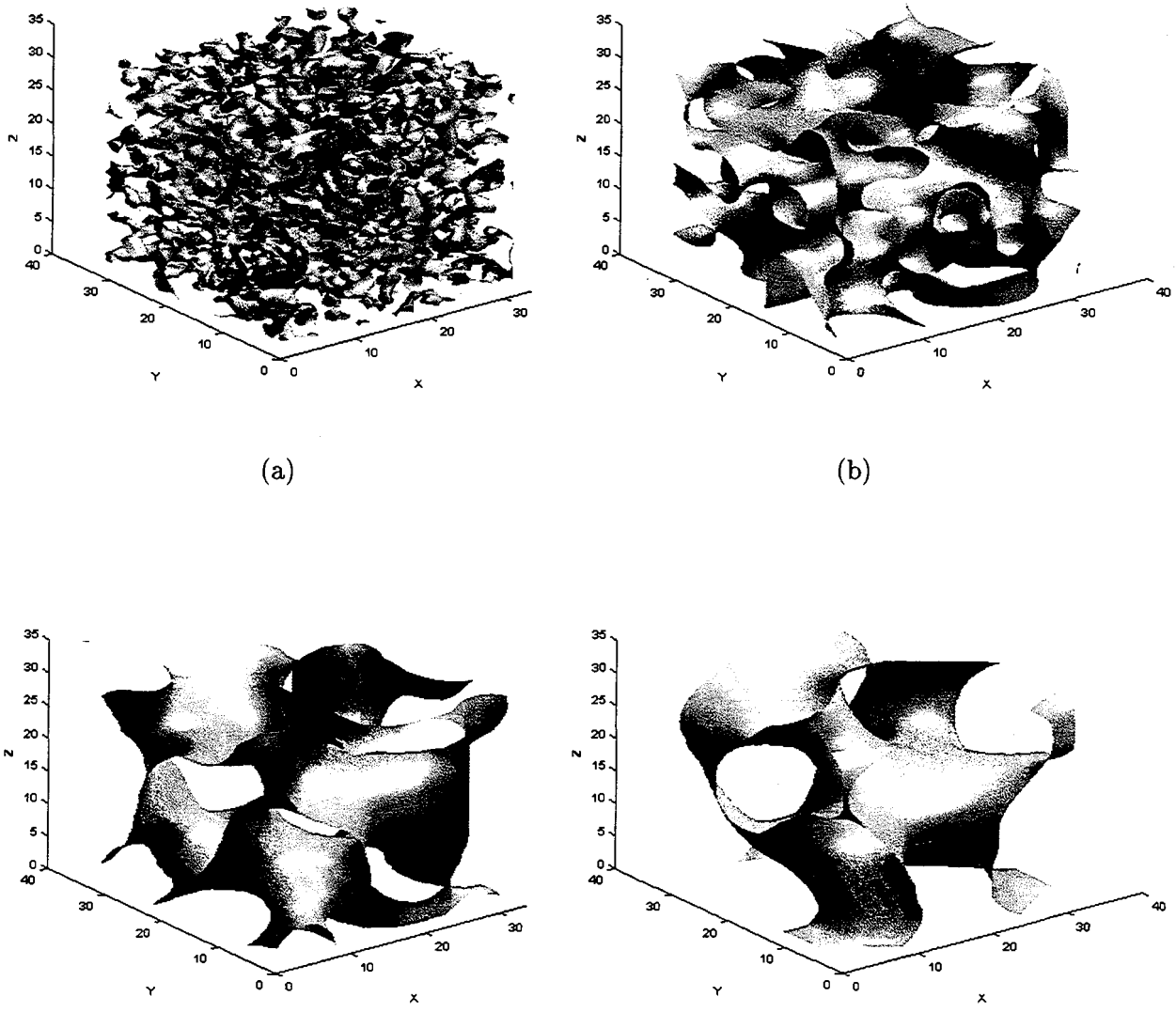

Figure 5.10: Evolution of u represented by the isosurfaces of separation of the two types of monomers at $u = 0$ at different time: $(a)t = 0.00469, (b)t = 7.57, (c)t = 45.42, (d)t = 98.41$. The mean value $m = 0, N = 32, \epsilon = 0.08, \sigma = 0, \Delta t = 0.0015$.

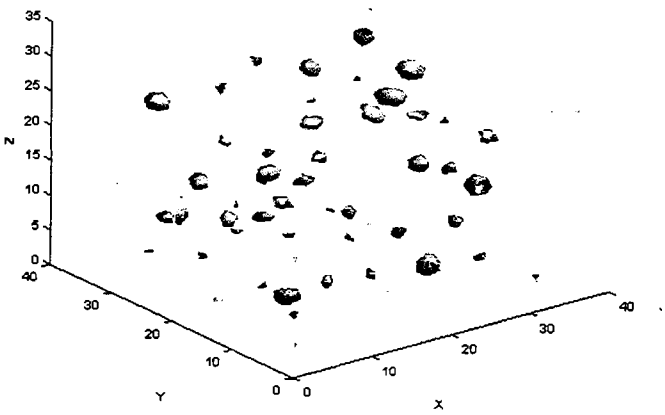

(a)

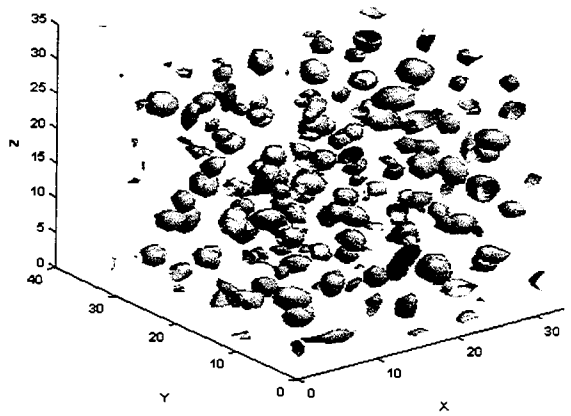

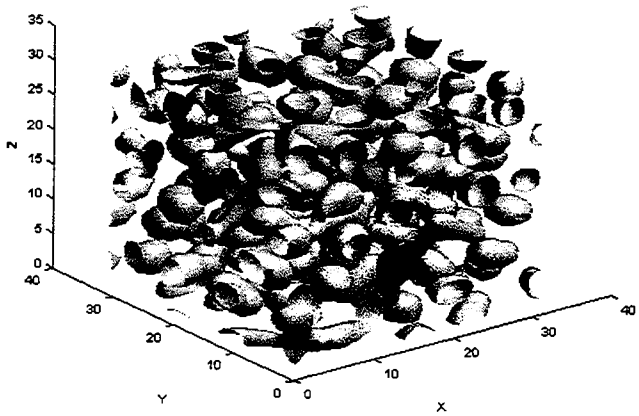

(c) (d)

Figure 5.11: Evolution of u in the first stage, during which the phase regions are formed, at different time: $(a)t = 0.6525, (b)t = 0.6979(c)t = 1.0159$. The mean value $u = 0.4, N = 32, \epsilon = 0.08, \sigma = 0, \Delta t = 0.0015$.

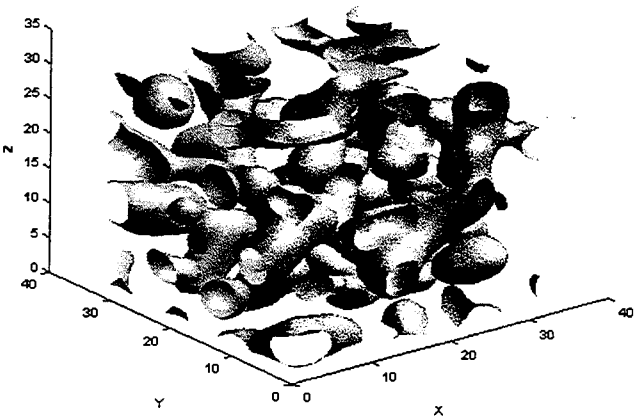

(a)

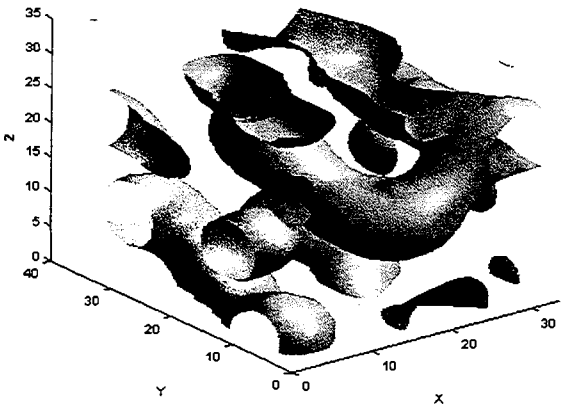

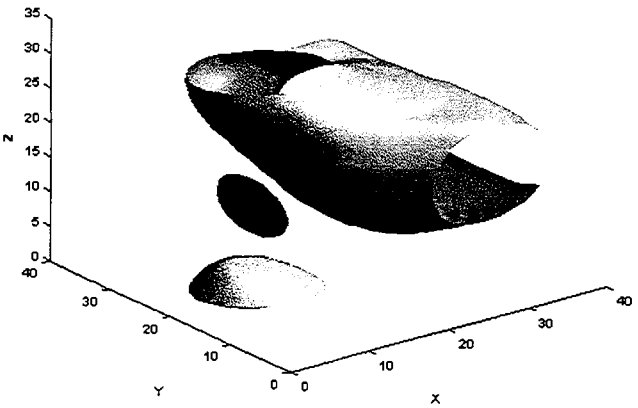

(c) (d)

Figure 5.12: Evolution of u in the second stage, during which the configuration of phase regions is coarsened, at different time: $(a)t = 3.029, (b)t = 15.14(c)t = 99.92$. The mean value $u = 0.4, N = 32, \epsilon = 0.08, \sigma = 0, \Delta t = 0.0015$.

85 – 100% S for B spheres in an S matrix.

The simplest of these ordered structures is the lamellar phase which is observed to occur when the volume fractions of the two monomers are comparable, Figure 5.13 (a). If the volume fraction of one monomer becomes larger than that of the other, the minority component is observed to form cylinders, Figure 5.13 (b). With increasing asymmetry in the volume fractions, spheres are generated.

The ordered phases are not limited to these structures. Later, several new phases were detected. However, it was not clear whether these new phases were thermodynamically stable.

5.4.2 The role of σ

Figure 5.14 shows the results with an increasing σ for the case of $m = 0$ and that of $m = 0.4$. For the case of zero mean value, we see, more lamella are shown in the minimizing structure when σ increases. The same happens in the case of nonzero mean values. The property that the nonlocal term favors oscillation is well validated by these numerical results.

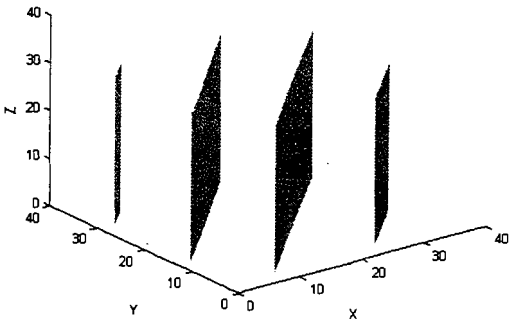

(a)

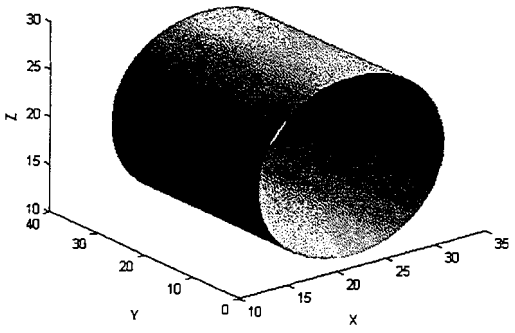

(b)

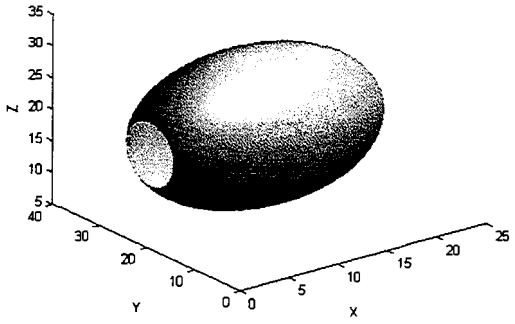

(d)

Figure 5.13: Stable state of u with different mean values: $(a)m = 0, (b)m = 0.4, (c)m = 0.5$. $N = 32, \epsilon = 0.08, \sigma = 0$.

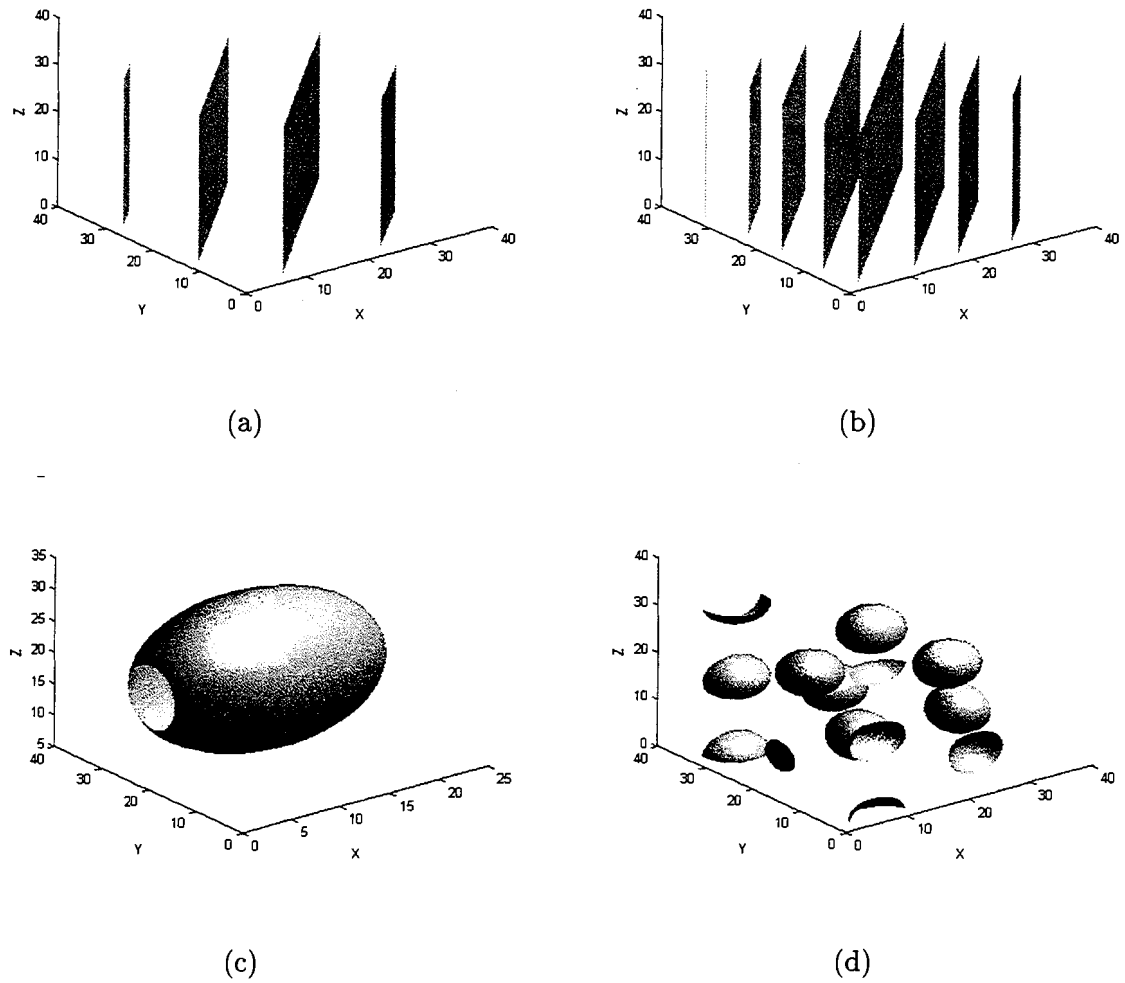

Figure 5.14: Stable states of u with different mean values and σ: $(a)m = 0, \sigma = 0.1, (b)m = 0, \sigma = 0.8, (c)m = 0.5, \sigma = 0.1, (d)m = 0.5, \sigma = 1.6. N = 32, \epsilon = 0.08, \Delta t = 0.0015$.

Chapter 6

Conclusions

In this thesis, we have studied the periodic phase separation numerically through the modified Cahn-Hilliard equation. This evolution equation was induced as a gradient flow for the nonlocal Cahn-Hilliard energy functional. The role of the three terms in this energy functional was discussed. The interfacial energy prefers small transition regions, while the double-well energy prefers pure phases to a mixture. The nonlocal term, however, favors oscillations around the mean value m. These three terms compete each other while the total energy is being minimized. Based on the role of each term and the mean value m, we examined the minimizing structures. Theoretically, periodic or nearly periodic structures are expected. And these anticipated periodic structures agree well with our numerical results.

The split-step pseudo-spectral method we used for numerical simulation is first order in time. This kind of time-splitting method is known as *Lie splitting*. Higher order split-step method like *Strang splitting*, which is second order in time, can also be considered. Our numerical scheme works well to some extend. However, we came up with blowups or unexpected results when the value of σ is too large. In fact minimizing structures in 3D are very complicated ([24]). Our code can only generate some simple structures. It is not powerful enough to capture all possible cases.

6.1 Future Work

There are many other interesting problems left to be investigated. The geometry of minimizing structures is affected by the nonlocal term as well. It has been theoretically pointed out, through the first variation of a nonlocal isoperimetic problem ([12]), that in two dimensional phase separation, except strips, minimizers will not have constant mean curvature. Numerical tests on this problem will be our future work. For the Cahn-Hillard equation, the asymptotic growth law of the characteristic domain size at late stages was found to be $t^{1/3}$ ([22] [23] [6] [7]). But for the nonlocal Cahn-Hilliard equation, the asymptotic growth law remains to be investigated.

Bibliography

[1] Badalassi, V.E., Ceniceros, H.D. and Banerjee, S.: Computation of multiphase systems with phase field models, *Journal of Computational Physics*, 190 (2003), 371-397.

[2] Bates, Frank S. and Fredrickson, Glenn H.: Block Copolymers-Designer Soft Materials, *Physics Today*, Feb. (1999), 32-38.

[3] Bloway, J.F. and Elliott, C.M.: The Cahn-Hilliard gradient theory for phase separation with non-smooth free energy, Part I: Mathematical analysis, *European Journal of Applied Mathematics*, Vol. 2 (1991), 233-279.

[4] Bloway, J.F. and Elliott, C.M.: The Cahn-Hilliard gradient theory for phase separation with non-smooth free energy, Part II: Numerical analysis, *European Journal of Applied Mathematics*, Vol. 3 (1992), 147-179.

[5] Cahn, J.W. and Hilliard, J.E.: Free energy of a nonuniform system I. Interfacial free energy, *Journal of Chemical Physics* 28(1958), 258-267.

[6] Chakrabarti, A. and Toral, R.: Late stages of spinodal decomposition in a three dimensional model system, *Physical Review B*, Vol. 39 (1989), 4386-4394.

[7] Chakrabarti, A., Toral, R. and Gunton, J.D.: Scaling behavior of a model of block copolymers in three dimensions, *Physical Review A*, Vol. 44 (1991), 6503-6507.

[8] Choksi, R.: Mathematical Aspects of Microphase Separation of Diblock Copolymers, Conference Proceedings, RIMS, Kyoto, Nov. 2002. *Surikaisekikenkyusko Kokyuroku*, Vol 1330 (2003), 10-17.

[9] Choksi, R. and Ren, X.: On the Derivation of a Density Functional Theory for Microphase Separation of Diblock Copolymers, *Journal of Statistical Physics*, Vol. 113 (2003), 151-176.

[10] Choksi, R.: Scaling Laws in Microphase Separation of Diblock Copolymers, *Journal of Nonlinear Science*, Vol. 11(2001), 223-236.

[11] Choksi, R. and Sternberg, P.: Periodic Phase Separation: the Periodic Cahn-Hilliard and Isoperimetric Problems, to appear in *Interfaces and Free Boundaries* (2006).

[12] Choksi, R. and Sternberg, P.: On the First and Second Variations of a Nonlocal Isoperimetric Problem, to appear in *Journal für die Reine und Angewandte Mathematik* (2006).

[13] Cowan, C.: The Cahn-Hilliard Equation as a Gradient Flow, *MSc. Thesis* (2005).

[14] Elliott, C.M.: Numerical Studies of the Cahn-Hilliard Equation for Phase Separation, *IMA Journal of Applied Mathematics* 38

[15] Grant, M., Miguel, M.S., Vinals, J. and Gunton, J.D.: Theoty for the early stages of phase separation: The long-range-force limit, *Physical Review B*, Vol. 31 (1985), 3027-3029.

[16] Kawasaki, K. and Ohta, T.: Equilibrium Morphology of Block Copolymer Melts, *Macromolecules* 19 (1986), 2621-2632.

[17] Kirkpatrick, S. and Stoll, E.: A Very Fast Shift-Register Sequence Random Number Generator, *Journal of Computational Physics*, Vol. 40 (1981), 517-526.

[18] Müller, S.: Singular perturbations as a selection criterion for periodic minimizing sequences, *Calculus of Variations* 1 (1993), 169-204.

[19] Muslu, G.M. and Erbay, H.A.: Higher-order split-step Fourier schems for the generalized nonlinear Schrödinger equation, *Mathematics and Computers in Simulation*, 67 (2005), 581-595.

[20] Ohnishi, I. and Nishiura, Y.: Some mathematical aspects of the micro-phase separation in diblock copolymers, *Physica D* 84 (1995), 31-39.

[21] Ohnishi, I., Nishiura, Y., Imai, M. and Matsushita, Y.: Analytical solutions describing the phase separation driven by a free energy functional containing a long-range interaction term, *Chaos*, Vol. 9 (1999), 329-341.

[22] Oono, Y. and Bahiana, M.: Cell dynamical system approach to block copolymers, *Physical Review A* Vol. 41 (1990), 6763-6771.

[23] Rogers, T. M., Elder, K. R. and Desai, R. C.: Numerical study of the late stages of spinodal decomposition, *Physical Review B* Vol. 37 (1988), 9638-9649.

[24] Teramoto, T. and Nisiura, Y.: Double Gyroid Morphology in a Gradient System with Nonlocal Effects, *Journal of the Physical Society of Japan*, Vol. 71 (2002), 1611-1614.

[25] Trefethen, Lloyd N.: Finite Difference and Spectral Methods for Ordinary and Partial Differential Equations, unpublished text, 1996, available at http://web.comlab.ox.ac.uk/oucl/work/nick.trefethen/pdetext.html